UPPSALA
UNIVERSITET

Digital Comprehensive Summaries of Uppsala Dissertations from the Faculty of Science and Technology 233

Development and Construction of a 2.5-MeV Neutron Time-of-Flight Spectrometer Optimized for Rate (TOFOR)

ANDERS HJALMARSSON

ACTA
UNIVERSITATIS
UPSALIENSIS
UPPSALA
2006

ISSN 1651-6214
ISBN 91-554-6686-9
urn:nbn:se:uu:diva-7198

Dissertation presented at Uppsala University to be publicly examined in Polhemsalen, Ångström Laboratory, Lägerhydssvägen 1, Uppsala, Friday, November 24, 2006 at 10:15 for the degree of Doctor of Philosophy. The examination will be conducted in English.

Abstract
Hjalmarsson, A. 2006. Development and Construction of a 2.5-MeV Neutron Time-of-Flight Spectrometer Optimized for Rate (TOFOR). Acta Universitatis Upsaliensis. *Digital Comprehensive Summaries of Uppsala Dissertations from the Faculty of Science and Technology* 233. 50 pp. Uppsala. ISBN 91-554-6686-9.

A new neutron time-of-flight spectrometer optimized for high count rate (TOFOR) has been developed for the JET research tokamak. TOFOR will measure the energy distribution of neutrons emitted from the d+d $\rightarrow$ ^{3}He+n fusion reactions in deuterium plasma. It will serve as the principal neutron spectroscopy diagnostic of high fusion power plasmas produced by injection of radio frequency waves (RF) and neutral beams (NB). The objective is to study plasma effects of RF and NB injection, with regard to temperature rise of the bulk deuteron population and the characteristics of supra-thermal components manifesting themselves over an extended energy range and with large spectral intensity variations.

To meet the plasma diagnostic objectives, special demands have been put on the design and characterization of TOFOR which, to a great extent, has relied on extensive neutron transport calculations. These calculations were used to optimize the design and to determine the TOFOR neutron response function. For the response function, TOF spectra were simulated for 81 quasi mono-energetic neutron energies in the range 1 to 5 MeV.

This thesis presents new results on instrumental solutions on the problem to reach high count rates, leading to a factor of hundred improvement compared to earlier designs.

With regard to the analysis of measured TOF spectra, the determined response function was folded with models and fitted to measurement data. The general issue of the energy dependence of the response function is raised and its importance is illustrated with analysis of high-quality TOF spectra for NB and RF heated plasmas. Potential for future developments are identified in the use of hybrid cards able to provide digital infromation on both time and pulse height.

Anders Hjalmarsson, Department of Neutron Research, Box 525, Uppsala University, SE-75120 Uppsala, Sweden

ISSN 1651-6214
ISBN 91-554-6686-9
urn:nbn:se:uu:diva-7198 (http://urn.kb.se/resolve?urn=urn:nbn:se:uu:diva-7198)

Till de som alltid stått vid sidan och givit sitt fulla stöd.
Mamma, Pappa, Peter, Mathz och Kjell

List of Papers

This thesis is based on the following papers, which are referred to in the text by their Roman numerals.

I **Comparision of neutron emission spectra for D and DT plasmas with auxiliary heating**
Giacomelli, L., Conroy, S., Ericsson. G., Gorini, G., Henriksson, H., Hjalmarsson, A., Källne. J. and Tardocchi, M., The European Physical Journal D **33** (2005) 235-241

II **Neutron time-of-flight spectrometer for high rate diagnosis of deuterium plasmas**
Hjalmarsson, A., Conroy, S., Ericsson, G., Gorini, G., Henriksson, H., Källne J. and Thun, J., Rev. Sci. Instr. **72**, No 1 (2001) 841-844

III **The TOFOR spectrometer for 2.5 MeV neutron measurements at JET**
Hjalmarsson, A., Conroy, S., Ericsson, G., Giacomelli, L., Gorini, G., Henriksson, H., Källne J., Tardocchi, M. and Weiszflog, M., Rev. Sci. Instr. **74**, No 3 (2003) 1750-1752

IV **Characterization of a scintillator detector with charged particles and pulse light emission**
Hjalmarsson, A., Conroy, S., Ericsson, G., Gatu Johnson, M., Giacomelli, L., Glasser, W., Gorini, G., Hellesen, C., Källne J., Ronchi, E., Sjöstrand, H., Sundén Andersson, E., Tardocchi, M., Thun, J. and Weiszflog, M., In manuscript.

V **Neutron transport simulations for the design and performance optimization of the TOFOR neutron time-of-flight spectrometer**
Hjalmarsson, A., Conroy, S., Ericsson, G., Giacomelli, L., Källne J., In manuscript.

VI **Response function simulation of the TOFOR neutron time-of-flight spectrometer**
Hjalmarsson, A., Conroy, S., Ericsson, G., Giacomelli, L., Källne, In manuscript.

Reprints were made with permission from the publishers.

Contents

1. Introduction

With ever increasing energy consumption in the world, new energy sources will be needed. One potential future candidate is thermonuclear fusion. In the case of fusion, the fuel and the material needed for reactor construction are in ample supply which could last for thousands of years. It is also an environmentally friendly energy source which will not release pollution, such as, greenhouse gases. Fusion is practically pollution free as the power production takes place within a closed system. Moreover, although it is a nuclear fuel that is used, there will be no radioactive waste from the fuel itself. Unfortunately, during the lifetime of a fusion power plant, the construction material of the reactor will be activated and must be handled as nuclear waste. In contrast to todays' fission reactors, this waste does not contain any actinides or fissile material. Finally, in contrast to fission, fusion reactors make use of the fuel through thermonuclear combustion. The fission is driven by the neutron flux around the fuel in the reactor core while it is the temperature of the fuel that drives a fusion reactor, so fusion reactor accidents cannot be catastrophic to the environment.

1.1 Fusion reactions

In order for a fusion reactor to work, the fuel particles have to overcome the repulsive Coulomb force acting between them. This is achieved by raising the fuel temperature to hundred million degrees Kelvin which corresponds to a particle kinetic energy of approximately 10 keV. This means that when the fuel is let into the reactor, as a gas, it is ionized and transformed to a plasma in which the electrons are decoupled form its nuclei. A thermonuclear fusion reactor is one in which the kinetic energy of the fuel ions must be a significant fraction of the repelling Coulomb force acting between them. For this reason one makes use of isotopes of the lightest element in the periodic table, i.e., deuterium (D) and tritium (T) of hydrogen. The most probable fusion reactions taking place in a D plasma are

$$d + d \rightarrow {}^{3}He + n + Q(3.27MeV) \tag{1.1}$$

$$d + d \rightarrow t + p + Q(4.03MeV) \tag{1.2}$$

and in a mixed D+T plasma,

$$d + t \rightarrow \alpha + n + Q(17.59MeV). \tag{1.3}$$

Here, Q is the mass difference between fuel ions and products, and it is also the free (kinetic) energy given to the products. The kinetic energy of the products is distributed according to their masses, so the neutrons in reaction 1.1 and 1.3 obtain a kinetic energy of approximately 3/4×Q = 2.45 MeV and 4/5×Q = 14.1 MeV, respectively. The remainder (0.8 and 3.5 MeV) is going to the charge particles while the full free energy is given to the charge particles in reaction 1.2. For the dd reactions in a D plasma, the reaction branching ratio is 50:50, so the average produced Q is 3.65 MeV of which 1/3 is carried by the neutron and the rest by the charged particles.

In order for a fusion reactor to operate at a power level of 1000 MW it will burn 11 mg/s of deuterium or 350 kg/yr. For comparison, we note that it would take 1.6 billion tons of coal and 4.4 billion tons of oxygen to produce the same amount of power per year [1]. Instead of a pure deuterium plasma, one can use a 50:50 DT mix. Such a reactor would require only 40 kg/yr and 60 kg/yr of D and T, respectively. The tritium has to be produced through breeding from lithium, i.e, the reactions $n + {}^6Li \rightarrow \alpha + t$ and $n + {}^7Li \rightarrow \alpha + n + t$. This, of course, is an extra complication. Still, a DT plasma is preferred as it requires a lower temperature to burn the fuel than a D plasma reactor. The benefit lies in the higher reactivity of dt than dd reactions for moderately high temperatures, i.e., ≤ 50 keV.

The reactivity is the product of the cross section and the relative ion velocity, $\sigma(v) \cdot v$, which for fusion reactions is an integral over the fuel ion velocity $\langle \sigma v \rangle$. As the velocity distribution in a fusion plasma is ideally Maxwellian (thermal condition), the reactivity is a function of ion temperature (T_i) and unique for the reactants involved. The dd and dt reactivities [1] differ both with regard to the shape of the temperature dependence but more important for fusion reactor application is the amplitude (Fig. 1.1). A comparison of $\langle \sigma v \rangle$ for the dd and dt reactions in a regime suitable for a reactor (around 10 keV and upwards) shows that the reactivity of dt is two orders of magnitudes higher than that of dd. This together with the fact that the Q-value is nearly 5 times higher makes DT the preferred fuel in a reactor. Besides temperature, the fuel density (n_f) is an principal characteristic of fusion plasmas. As the reactivity, is given in units of cm^3/s one would, for a DT plasma, obtain the reaction rate density $\mathrm{R}_f = \mathrm{n}_d \cdot \mathrm{n}_t \cdot \langle \sigma v \rangle \ \mathrm{cm}^{-3} \cdot \mathrm{s}^{-1}$ and with $\mathrm{n}_d = \mathrm{n}_t = \mathrm{n}_f/2 = 10^{14} \ \mathrm{cm}^{-3}$ one would obtain $\mathrm{R}_f = 10^{12} \ \mathrm{cm}^{-3} \cdot \mathrm{s}^{-1}$ if $\mathrm{T}_i = 10$ keV, i.e., 1 % of the fuel would be burnt per second. To obtain the same fuel burn ratio in a D plasma, it is not enough to raise the temperature to impractically high values (Fig. 1.1) but also a higher density would be required. As hydrogen plasmas have a week isotopic dependence, it is equally difficult to create a stable equilibrium condition for high values of temperature and density. The DT plasma is thus preferable in a fusion reactor for the reasons mentioned. On the other hand, many of the plasma aspects of a fusion reactor can be studied in D plasmas.

[1] The estimate is based on a released energy of 2.3 eV for $\mathrm{C} + \mathrm{O}_2 \rightarrow \mathrm{CO}_2$.

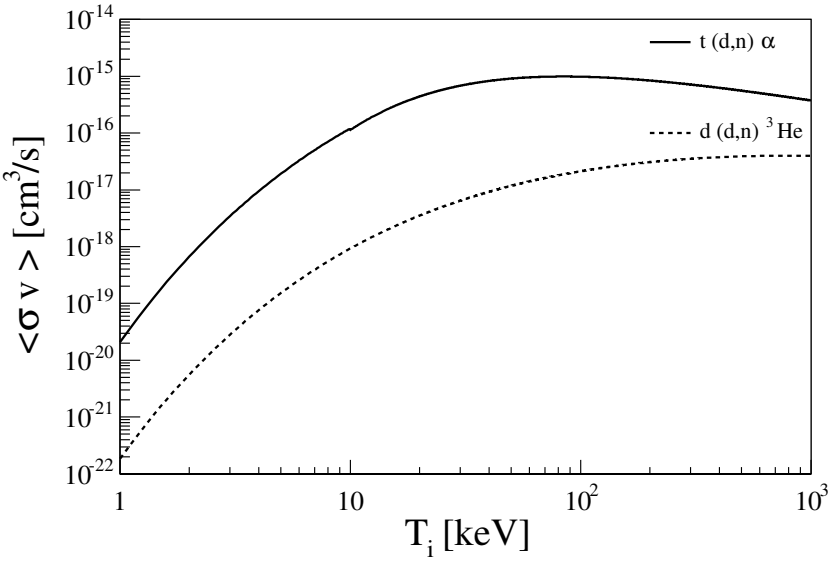

Figure 1.1: Reactivity, $\langle\sigma v\rangle$, for the two fusion reactions t(d,n)α and d(d,n)^{3}He as function of plasma ion temperature, T_i.

As it is simpler to perform experiments with D plasmas, these are the ones presently used in today's fusion experiments.

There are other fusion fuel aspects to consider such as radiation effects on the reactor. A reactor with DT fuel will produce a harder neutron emission spectrum than a D fueled one, both with respect to kinetic energy (14.1 compared to 2.5 MeV) and the carried fraction of released power (80 and 34 %, respectively). This implies a drawback in terms of higher activation of a DT fueled reactor compared to one with D. Moreover, T is an unstable isotope with a half life of around 12 years which demands a special enclosure and gas handling system, and implies an extra contamination locally in the vessel of the reactor. Due to the contamination and handling problems with the use of T, it is only used at JET among todays' research reactors. However, most experiments in JET, and other magnetic confinement experiments, use deuterium for the base plasma.

With regard to the radiation problems mentioned above, one can consider using a fuel which releases no neutrons when burnt. One such example is $\mathrm{d} + {}^3\mathrm{He} \rightarrow \alpha + \mathrm{p}$. It is the analogue of $\mathrm{d} + \mathrm{t} \rightarrow \alpha + \mathrm{n}$ but for its much lower reactivity at given T_i. It is true that the plasma facing wall would be spared from the neutron activation but all the fusion power would be absorbed in the surface layer of the walls resulting in five times higher heat load compared to a DT reactor. In the latter case, most of the power is carried by the neutrons and deposited over a certain depth, i.e., volume absorption of the heat. Besides being an energy carrier, the neutrons also carry much of the so called diagnos-

tic information about the plasma, specifically, on the fuel burn process in it. It is this aspect this thesis is concerned with.

1.2 Magnetic confinement

In order for fusion reactions to take place, a plasma with a temperature of a few keV has to be produced. To sustain this temperature and to protect the reactor, the plasma must be insulated from its surrounding vessel walls. Since the plasma consists of charged particles, the insulation can be accomplished by the use of strong magnetic fields so that the plasma can be contained as in a 'bottle'. There exist many magnetic confinement configurations of which we mention two here, namely, the stellarator and the tokamak [2]. Both are toroidal devices but differ in the way that one of the confining magnetic fields is generated, namely, the polodial one. In the stellarator external coils are used to produce both the toroidal and poloidal magnetic fields to form the needed helical field spiraling around the tours. In a tokamak the poloidal field is produced by a toroidal current driven through the plasma. The poloidal field component is essential to achieve a plasma equilibrium state under which the plasma pressure is balanced by the magnetic counter force. A schematic picture of toroidal, poloidal and the resulting helical magnetic fields for the tokamak configuration is shown in Fig. 1.2. Of the two reactor types mentioned, the tokamak is the most studied and successful so far. The largest tokamak in the world today is the Joint European Torus (JET) [3]. It will be followed by an even larger one, ITER [4].

1.3 The JET tokamak

The European tokamak JET is located at the Culham laboratory site, south of Oxford, England. The construction of JET started in 1979 and the first plasma was produced in 1983. Since then, a large number of different experiments have been carried out with the aim to investigate confinement and heating of the plasma, plasma vessel wall interactions and the release of impurities, etc. Three DT experimental campaigns have been carried out to study how α-particles affect the plasma. To fulfill the aims, the machine is equipped with auxiliary heating systems in the form of neutral beam (NB) injection, ion cyclotron resonance heating (ICRH) with radio frequency (RF) waves and lower hybrid current drive (LHCD) heating. For the NB heating system, neutral atoms of typical energies of 80 keV (up to 130 keV) are injected into the plasma. When reaching the plasma the atoms will be ionized and confined in the tokamak. These NB generated fast ions will form a supra-thermal population in the plasma and slow down through (small angle) Coulomb interactions

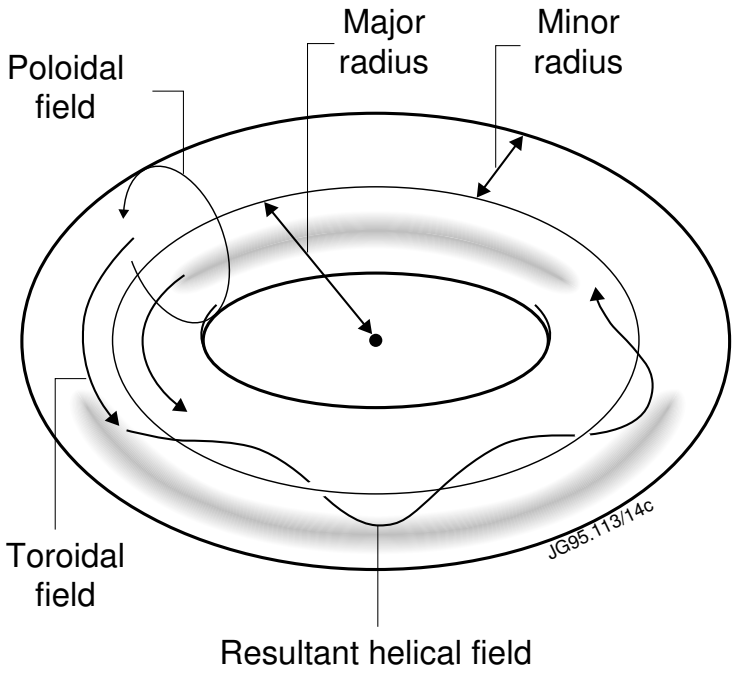

Figure 1.2: Schematic picture of the magnetic fields generated in a tokamak. A toroidal field generated with external coils and a poloidal field by transformer action. A superposition of the two fields results in a helical field, spiraling around the torus, used for confinement of the plasma.

thus heating the plasma[2]. The power that can be injected from the NB system is about 22 MW. In the case of ICRH, electromagnetic waves launched into the plasma have a frequency tuned to the cyclotron resonance of a specific ion species confined in the plasma of a certain magnetic field value. The energy of the RF waves will be transfered to the plasma, for instance, through the drag exerted by the plasma to the ICRH accelerated ions. The maximum power that can be launched by ICRH is approximately 32 MW, but the fraction that can be deposited in the plasma is often limited by plasma coupling factors. In the case of LHCD, microwaves are emitted into the plasma and will "push" the confined electrons in a certain direction generating a current that will also heat the plasma [5]. The maximum power available for LHCD is of the order of 6 MW. The basic heating of the plasma is always produced by the current induced in order to create the poloidal magnetic field; this together with the plasma resistivity will produce Ohmic heating up to 3 MW for the JET tokamak.

[2]A small fraction of ions from NB can also burn-up in fusion reactions before they have been thermalized (through head-on collisions with thermal fuel ions in the bulk). These supra-thermal reactions give rise to neutrons of a velocity distribution peculiar to their source.

In a fusion reactor, it is the α-particles that will be the essential part of the plasma heating with amounts up to one fifth of the fusion power, i.e., $P_\alpha = P_f/5$ where $P_f = P_\alpha + P_n$. To study the effect of α-particles, the first main DT campaign (DTE1) was conducted in 1997 [6]. During this campaign a new world record in produced P_f was achieved, resulting in a P_f=16.1 MW. A new record in total fusion energy in one discharge was also achieved and set at 21.7 MJ for a plasma generating 4.5 MW of fusion power over a period of approximately 5 s.

Part of the JET experimental progress is assessed based reaching ever higher performance. To this end, an enhanced performance (EP) program was started in 2000. This entailed more auxiliary heating power and new diagnostics [7]. On the diagnostic side, one of the accepted projects was the proposal to develop and construct a new instrument for neutron emission spectrometry (NES) diagnosis of D plasmas. This project was entitled the "time-of-flight optimized rate" neutron spectrometer diagnostic (TOFOR) [8]. This thesis is about the TOFOR design, construction and installation at JET.

1.4 The research of the present thesis

This thesis work began at the end of 1999 on simulation and test tools for the development of neutron diagnostics for fusion plasmas, with a main focus on the new neutron time-of-flight spectrometer optimized for high rates (TOFOR). This included initial neutron transport calculations to quantify the specifications of a TOFOR spectrometer based on conceptual estimates [9]. The simulation programs were developed into a full model of the TOFOR system which was used in the design phase, and later on, for neutron response function calculations.

The design and construction phase also required laboratory tests of the scintillation detectors used in TOFOR. For this purpose a test facility was built up including development of software for control systems such as xy-tables and electronics to acquire data.

Work on the construction of TOFOR started after it had been approved as one of the projects in the JET enhanced performance program. The decision came very suddenly in May 2002 and a tight deadline for delivery was set to May 2004. The schedule was revised according to which TOFOR was to be delivered to JET January 2005 and subsequently installed and commissioned. The first neutrons were recorded in November 2005 when JET started up after a long shut down period. The first dedicated experiment was conducted in May 2006.

This thesis was done as part of the large TOFOR project conducted by an international team involving some twenty scientists. My contributions include most of the technical aspects of the project as well as the preparation phase

that started in 1999. Some of the work is presented in the papers included in this thesis where I carried the principle responsibility (except paper I). This concerns the description of the neutron response of the TOFOR spectrometer and setting up and performing some of the test experiments in order to describe the pulse response of the scintillators that TOFOR is based on. It should be noted that the neutron transport simulations were performed to the level of detail and extension which provided the underlying knowledge to describe the neutron response function over an amplitude range of 1 to about 10^{-4} for the energy range $E_n = 1$ to 5 MeV. This represents the most advanced description of a TOF spectrometer for fusion neutrons undertaken up till now and was made to match the envisaged high observational capability of the TOFOR instrument.

2. Spectrum of neutron emission from deuterium plasmas

2.1 Kinematics of fusion neutrons from thermal plasmas

Derivation of the kinetic energy released to the neutrons generated in the fusion reactions 1.1 and 1.3 have been performed in Ref. [10]. For the reaction $\mathrm{d}+\mathrm{d} \rightarrow {}^3\mathrm{He}+\mathrm{n}$ it is given by

$$\begin{aligned} E_n &= \frac{1}{2} m_n V_{CM}^2 + \frac{m_{^3He}}{m_{^3He}+m_n}(Q+K) \\ &\quad + V_{CM}\cos(\theta)\sqrt{\frac{2m_{^3He}m_n}{m_{^3He}+m_n}(Q+K)} \end{aligned} \tag{2.1}$$

where $m_{^3He}$ and m_n are the masses of the reaction products, Q is the mass difference of the reactants and products, $\mathbf{V}_{CM}$ is the velocity of the center of mass derived by

$$\mathbf{V}_{CM} = \frac{m_d \mathbf{v}_{d_1} + m_d \mathbf{v}_{d_2}}{2m_d} = \frac{\mathbf{v}_{d_1} + \mathbf{v}_{d_2}}{2} \tag{2.2}$$

where m_d is the deuteron mass, $\mathbf{v}_{d_1}$ and $\mathbf{v}_{d_2}$ are the velocities of the reacting deuterons and K is the relative kinetic energy of the reacting particles given by

$$K = \frac{1}{4} m_d \mathbf{v}_{rel}^2. \tag{2.3}$$

Here m_d is the deuteron mass and $\mathbf{v}_{rel}$ the relative velocity between the reacting deuterons. In the last term of eq. 2.1, the factor $V_{CM}\cos(\theta)$ represents the component of $\mathbf{V}_{CM}$ in the direction of the neutron velocity vector, $\mathbf{u}_n$, in the center of mass system. If the reactants are isotropically distributed, which is the case for a plasma in thermal equilibrium, i.e, the reacting deuterons are Maxwellian distributed, the term with $V_{CM}\cos(\theta)$ vanishes because the average of $\cos(\theta)$ is zero. Hence, for a plasma in thermal equilibrium the mean neutron energy $\langle E_n \rangle$ is given by

$$\begin{aligned} \langle E_n \rangle &= \frac{1}{2} m_n \langle V_{CM}^2 \rangle + \frac{m_{^3He}}{m_{^3He}+m_n}(Q+K) \\ &= E_0^{dd} + \frac{1}{2} m_n \langle V_{CM}^2 \rangle + \frac{m_{^3He}}{m_{^3He}+m_n}\langle K \rangle \\ &= E_0^{dd} + \Delta E_{th} \end{aligned} \tag{2.4}$$

Table 2.1: *The width ΔE_n (FWHM) as function of T_i for two fusion reactions with a neutron as one of the products.*

Reaction	ΔE_n
d(d,n)^{3}He	$82.5\sqrt{T_i}$
d(t,n)α	$177\sqrt{T_i}$

with a numerical value of E_0^{dd}=2.449 MeV taken from Ref. [11] and as given by the reaction Q-value and the masses of the reaction products. The E_0^{dd} value will also define the neutron mean energy peak position in the limit of a zero-degree plasma, i.e.,

$$T_i = 0 \Rightarrow \begin{cases} \mathbf{V}_{CM} = 0 \\ \langle K \rangle = 0 \end{cases}$$

The second term ΔE_{th} in eq. 2.4, is a shift of the mean (peak) neutron energy for plasmas of $T_i > 0$. This shift has been calculated in Ref. [12] as function of T_i, showing that the magnitude of the shift is of the same order as T_i for different fusion reaction channels, i.e., a peak shift of $\Delta E_{th} \approx 32$ keV is introduced for a thermal plasma with an ion temperature of T_i = 10 keV for the reaction d(d,n)^{3}He. Moreover, the width, ΔE_n (FWHM), of the resulting neutron energy distribution can be calculated from the velocity distribution of the reactants.

For a thermal plasma, the ion velocity distribution is given by a Maxwellian that is only dependent on ion temperature T_i and given by

$$f(\mathbf{v}_X) = \left(\frac{m_X}{2\pi T_i}\right)^{\frac{3}{2}} \exp\left(-\frac{m_X v_X^2}{2T_i}\right). \tag{2.5}$$

For the operational regime of a tokamak, $T_i \ll Q$, the resulting neutron energy distribution is given by a Gaussian

$$f_n(E_n) = \frac{1}{\sigma\sqrt{2\pi}} \exp\left(\frac{(E_n - E_0)^2}{2\sigma^2}\right), \tag{2.6}$$

whose width (FWHM) can be expressed as

$$\Delta E_n = 2\sqrt{\ln(2)}\sigma = 2\sqrt{\frac{\ln(2) 4 m_n E_0^{dd} T_i}{2 m_d}} \tag{2.7}$$

for the reaction d(d,n)^{3}He; its relationship to T_i is shown in Table 2.1 in comparison to that for the dt reaction.

2.2 Rotating thermal plasmas

For a plasma experiencing a collective motion, for instance in the form of toroidal rotation, the emitted neutrons will be affected by a Doppler shift. This means that the neutron energy distribution is shifted and the E_n peak value is changed in proportion to $\pm\Delta E_R$ to be added to the right hand side of eq. 2.4. The Doppler shift can thus be observed in NES diagnosis of the plasma [13] depending on the angle between the velocity vector, $\mathbf{V}_C$, for the ion motion distribution and the line of sight of the spectrometer. For instance the full shift of $\pm\Delta E_R$ is seen for parallel or anti parallel directions and 70 % of the shift for a 45 degree angle. The effects on the neutron emission spectrum due

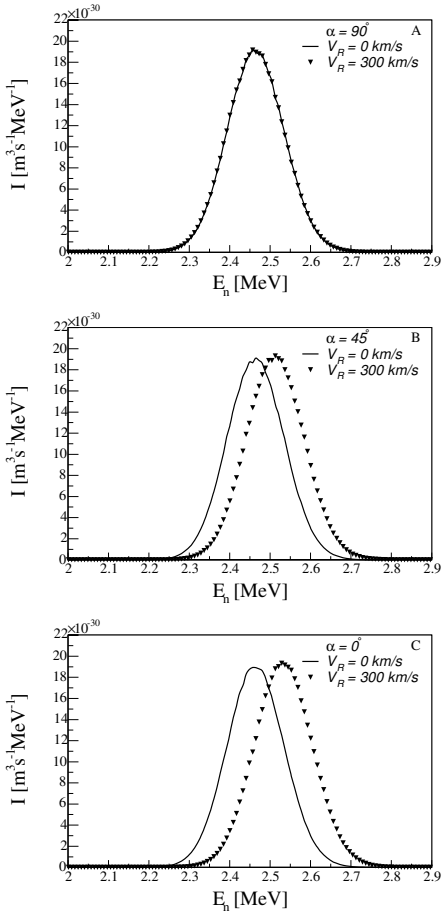

Figure 2.1: Point calculations of neutron energy spectra, showing peak shift, ΔE_{th}, due to a 4 keV ion temperature and plasma rotation. In all figures the line represent a 4 keV plasma with no rotation, the triangles is the same plasma rotating with a velocity V_R = 300 km/s and α is the angle between V_R and the line of sight of the instrument performing the measurement. (A), (B) and (C) represent different α's showing that a shift due to rotation can be measured if $\alpha \neq 90°$.

to plasma rotation are illustrated by the simulation results presented in Figs. 2.1A-C for three different angles (α) between $\mathbf{V}_C$ and the spectrometer line of sight.

Specifically, a rotation of 300 km/s gives a up/down Doppler shift of $\Delta E_R = 70$ keV for $\alpha = 0/180$ degrees compared to a Doppler broadening of 165 keV (FWHM) for 2.5-MeV dd neutrons. Doppler shifts can, in principle, be detected down to a fraction of the Doppler broadening.

2.3 Auxiliary heated plasmas

With the use of auxiliary heating, the neutron energy distribution given by eq. 2.6 is no longer valid as the heated plasma particles will be perturbed from their thermal equilibrium. This perturbation will result in a change of the velocity distribution of the heated particles which may result in a Maxwellian with a different T_i or a non-Maxwellian distribution for supra-thermal (slowing down) particles in general. For all these perturbed velocity distributions, one can use numerical methods to simulate the resulting neutron emission spectra which can be used as predictions for comparison with measurements. For this purpose, computer codes have been developed such as 'Cauldron' [14] and 'FPS' [15] to predict the neutron emission spectrum for assessment studies of ion velocity distributions.

Often one tries to parameterize the ion velocity distributions to facilitate fitting to the data. For instance, the temperature (T_{RF}) can be used to calculate the neutron emission from RF heating and the maximum beam energy (E_{NBI}) in the case of NBI. As an illustration of how different heating methods will effect the neutron emission spectra, calculations of RF and NBI heating were performed for the reaction d(d,n)^{3}He. The results are shown in Fig. 2.2 in comparison to the neutron emission spectrum of a thermal plasma. In the calculations, the heated particles were given a temperature of T_{RF} = 40 keV for RF and a maximum beam energy of E_{NBI} = 40 keV for the NBI. In order to compare the results, the RF and NBI components were normalized to each other with the assumption that 5 % of the deuterium population was affected by the heating. It was also assumed that the heated particles interacted only with the thermal bulk of the plasma (95 %) of T_i = 4 keV.

The results demonstrate that plasmas subjected to RF or NBI heating give neutron emission spectra that are no longer of Gaussian shape. Moreover, the spread in energy of the emitted neutrons will be broader compared to that of a thermal plasma. This is clearly the case for a bulk with T_i = 4 keV, but is generally true as T_i is typically no higher than 20 keV, and usually not above 10 keV at JET.

The values of T_{RF} = 40 keV and E_{NBI} = 40 keV used above, for purpose of illustration, are below typical values for experiments performed at JET. This implies that for NES diagnosis of JET plasmas one has to be prepared

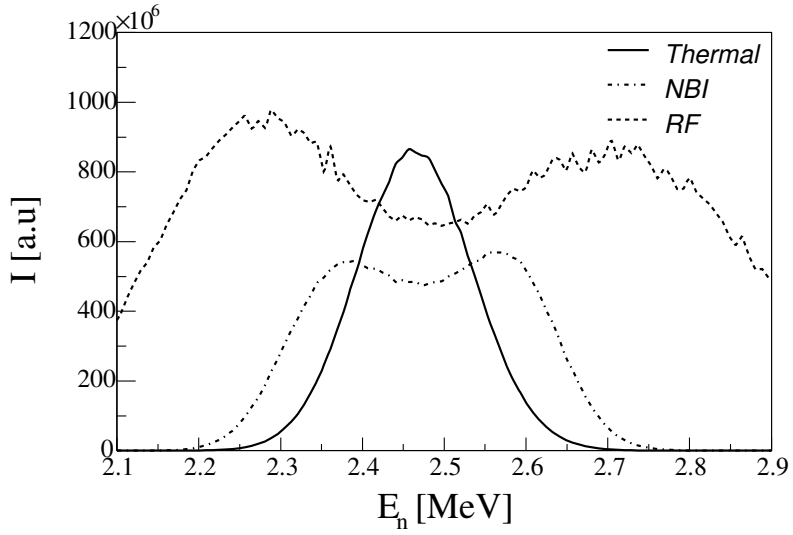

Figure 2.2: Point calculations of neutron spectral components generated by RF (dash) and NBI (dash dot) heating for the d(d,n)^{3}He fusion reaction for a radial line of sight. In the calculations it was assumed that the heated particles only interacted with a $T_i = 4$ keV thermal bulk plasma (full line) and that only 5 % of the total deuterium population was effected by the RF or the NBI heating.

to measure the neutron spectrum for d(d,n)^{3}He over the energy interval of say 1 - 5 MeV (paper I). This is a tough requirement on broad band neutron spectrometer. It also means that the response to neutrons over the same energy range must be determined (paper VI).

3. Neutron emission spectroscopy for fusion plasmas

Detection of neutrons requires nuclear reactions or scattering resulting in charge particle or ion recoil production, respectively. Examples of the former of interest for fusion neutron spectrometry are, for instance, ^{3}He(n,p)t [16, 17], ^{6}Li(n,α)t and ^{12}C(n,α)^{9}Be [18, 19], etc. In these reactions, the target nuclei are also part of the detector in which the charged products will deposit their energy given to them in full by the incoming neutron.

The principle of recoil detection is generally based on neutron scattering in a material containing hydrogen producing recoil protons, i.e., n+p$_H$ $\rightarrow$ n'+p. If the recoil proton is produced at a known angle, the neutron energy is uniquely related to the measured proton energy. The recoil energy can be obtained from measurement of pulse height [20] of the stopped proton, or, of its momentum using the Magnetic Proton Recoil (MPR) technique [21]. The MPR is an important high performance spectrometer and a prime choice for NES diagnosis of DT plasmas.

None of the above mentioned methods is the optimum choice for D plasmas. However, proton recoils is the base for the design of a 2.5-MeV dd neutron spectrometer. One possibility is the use of organic scintillators, in which recoil protons can be produced and detected *in situ*. However, a scintillation detector by itself does not provide sufficient information for measurement of the neutron spectrum. That is, neutrons of given energy produce a recoil energy distribution over the range $0 \leq E_p \leq E_n$ where each E_p is connected with a pulse height distribution. The relationship between recorded (pulse height distribution) data and the spectrum of the incoming neutron flux is complex and there is no one-to-one correspondence between them. An alternative way to use scintillators is to produce a n+p$_H$ $\rightarrow$ n'+p scattering and then record the scattered neutron n' when it passes a second detector. The two scintillation detectors (S1 and S2) define the scattering angle (α) for a neutron detected in both and also the flight time. This instrument is referred to as the neutron time-of-flight (TOF) spectrometer and it is identified as the technique most useful for NES diagnosis of D plasmas such as those produced at JET.

3.1 Time-of-flight

In order to be able to perform TOF measurements, the signals in the two scintillators S1 and S2 must be recorded whose times t_1 and t_2 can be related to the same neutron. This means that the scattered neutron has traveled the distance L from A to B in Fig. 3.1 with recorded "start" and "stop" times of t_1 and t_2. In a fusion experiment, the flux of neutrons is continuous over time

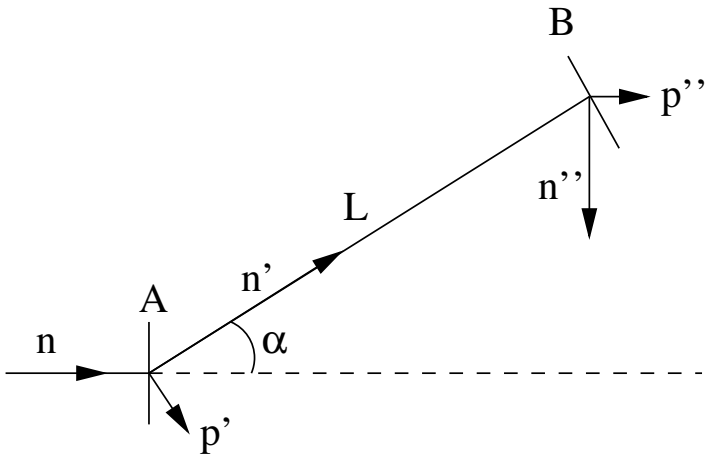

Figure 3.1: Schematic picture of a time-of-flight system, a incoming neutron (n) interact via proton elastic scattering at point A with a scattering angle α and the recoil proton (p') will generate a start signal for the TOF measurement (t_{start}). At point B the scattered neutron (n') interact ones more via proton elastic scattering and the recoil proton (p") provides a stop signal (t_{stop}). Hence, the t_{TOF} over the flight path L, for (n'), is given by $t_{TOF} = t_{stop} - t_{start}$.

periods of seconds up to minutes and the signal rates in S1 and S2 can be high. This means that one cannot know *a priori* which recorded time pairs t_1 and t_2, within a certain interval, are start and stop times for a neutron passing both S1 and S2, thus representing a valid TOF, and which are due to unrelated neutron events (spurious pairs). The measured $t_2 - t_1$ event distributions containing both real and spurious neutron pair events are referred to as t_{TOF} spectra.

Using the scattering kinematics shown in Fig. 3.1, the energy of the scattered neutron (n') $E_{n'}$ is given by

$$E_{n'} = \frac{1}{2} m_n v_{n'}^2 = \frac{1}{2} m_n \left(\frac{L}{t_{TOF}} \right)^2 \tag{3.1}$$

with m_n the neutron mass, $\mathbf{v}_{n'}$ the velocity of n' and t_{TOF} the flight time of n' for a fixed flight distance L. For n+p elastic scattering the incoming neutron

energy, E_n, can be obtained from $E_{n'}$, as disused in Ref. [22], by

$$E_n = \frac{E_{n'}}{\cos^2(\alpha)} \tag{3.2}$$

where α is the neutron scattering angle.

Building an instrument based on the configuration outlined in Fig. 3.1, consisting of two scattering points fixed in space relative each other, is not practical. For one thing, the detection efficiency will be very modest due to a very small solid angle for catching the scattered neutrons. Therefore, the geometry of the scintillators, especially S2, is essential to obtain high detection efficiency and, generally, to optimize the performance of the TOF spectrometer for measurements of fusion neutrons.

3.2 Constant time-of-flight

An increase of the solid angle for a neutron TOF spectrometer can be obtained if L is not of fixed in length but instead made to vary with the scattering angle, $L(\alpha)$. Defining $L(\alpha)$ as the distance between two scattering points on the circumference of a circle (point A and B in Fig. 3.2) with a fixed radius (R), L^2 can be expressed as

$$L^2 = 2R^2(1-\cos(\pi-2\alpha)) = 4R^2\cos^2(\alpha). \tag{3.3}$$

from which $E_{n'}$ can be expresses as

$$E_{n'}(\alpha) = \frac{1}{2}m_n v_{n'}^2 = \frac{1}{2}m_n\left(\frac{L(\alpha)}{t_{TOF}}\right)^2 = 2m_n R^2\frac{\cos^2(\alpha)}{t_{TOF}^2} \tag{3.4}$$

by combining eqs. 3.3 and 3.1. Assuming that the first n+p scattering of the incoming neutrons takes place at a fixed point on the circle and that the velocity vector for these incoming neutrons point toward the center of the circle, the incoming neutron energy is given by eq. 3.2. The result of eq. 3.4 together with 3.2 gives the incoming neutron energy as

$$E_n = \frac{2m_n R^2}{t_{TOF}^2}. \tag{3.5}$$

Thus, E_n is independent of scattering angle. In principle, all points on the circumference can be used to determine the incoming neutron energy which will dramatically increase the detection efficiency of the spectrometer compared to that of a fixed scattering angle configuration shown in Fig. 3.1.

With the above assumptions of the incoming neutrons and definition of $L(\alpha)$, the neutron flight time will be a constant independent of scattering angle for mono-energetic neutrons. This implies that there will be a one-to-one

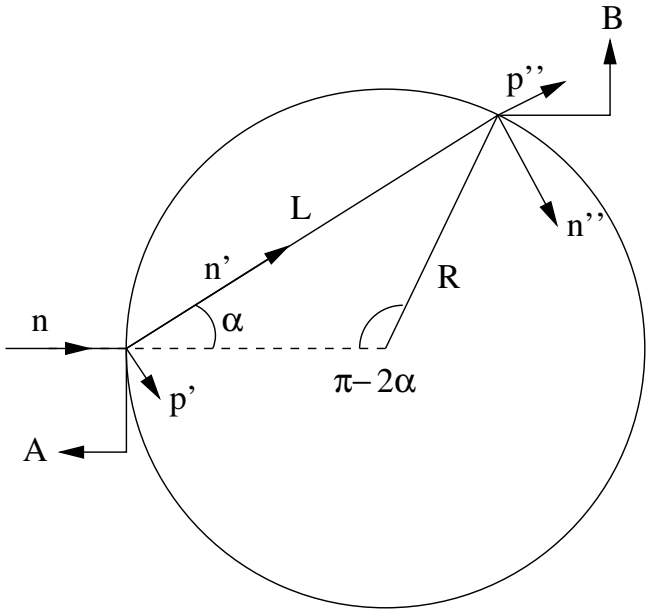

Figure 3.2: Schematic picture of a constant time-of-flight system, a incoming neutron (n) interact via proton elastic scattering at point A on the circumference of a circle with radius, R. The scattered neutron, (n'), interact via proton elastic scattering at a point B also positioned on the circumference of the circle. Hence, the neutron flight path, $L(\alpha)$, will be a function of scattering angle which together with neutron scattering kinematics will give a constant neutron flight time independent of α for mono-energetic incoming neutrons.

correspondence between the measured t_{TOF} distribution and the E_n distribution. By symmetry the above arguments are also valid in three dimensions and the circle will change in to a sphere. This has given rise to the concept of a constant time-of-flight sphere which is the preferred choice of geometry for a neutron TOF spectrometer used for diagnosis of deuterium fusion plasmas.

3.3 TOF spectrometers for diagnosis of deuterium plasmas

To perform neutron spectroscopy of a fusion plasma, neutrons emitted from a certain volume of the plasma are selected by a collimator. The collimation also defines the spectrometer's line-of-sight and creates a beam of neutrons of well defined direction as well as the cross section specifying the flux of the beam. The neutron flux will imping on the target detector S1 of the spectrometer

situated on the surface of the above discussed constant TOF sphere (point A in Fig. 3.2). A fraction of the incoming neutrons will interact in S1 through n+p scattering and generate recoil protons which will be detected to provide one of the signals used for the TOF measurement. A part of the scattered neutrons will have a scattering angle within the solid angle defined by the area of a second detector (S2). This detector is also situated on the surface of the TOF sphere (e.g, point B in Fig. 3.2) and will provide the second signal for the TOF measurement. This signal is also produced by recoil protons from n+p scattering but here at an angle suitable for neutron detection. To maximize the n+p scattering probability in both detectors, scintillators with a high hydrogen content, typically with a H:C ratio of 10:9, should be used. Moreover, since the signals are used to perform a time coincidence measurement the timing properties of the detectors are also essential. Plastic scintillators fulfill the above criteria and are therefor often the preferred choice of material in neutron TOF spectroscopy.

High hydrogen content is just a first step to achieve a TOF spectrometer with a high detection efficiency, ε. Another aspect is large scintillator volumes. For instance, for given neutron beam cross section, the thickness of S1 should be large to increase the fraction of scatterings. The same is true for S2, but it should also have a large area to increase the solid angle for catching scattered neutrons coming from S1. However, with large thicknesses, an uncertainty, ΔL, in the length of the scattered neutron flight path L will be introduced. ΔL is one of the factors that will contribute to the time resolution, Δt_{TOF}, of the t_{TOF} measurement so that high efficiency comes at the expense of time resolution, i.e., energy resolution of the neutron spectrum that one wants to measure (eq. 3.5). An objective for designing a TOF spectrometer is to find an optimized trade-off between ε and Δt_{TOF} for the application at hand.

Neutron TOF spectrometers, built to perform measurements of the 2.5-MeV neutrons emitted from D plasmas have been used on both the two large tokamaks in operation, JET and JT-60 [23]. These were based on the constant TOF sphere geometry but realized in different ways. The JT-60 spectrometer used a bent S2 scintillator to conform to the spherical geometry. Its specifications, as obtained from simulations, were a flux detection efficiency, $\varepsilon \approx 0.03$ cm^2 for 2.5-MeV neutrons and an energy resolution of $\Delta E_n/E_n \approx 3.2$ % [24]. The JET spectrometer used 12 scintillators (area of 78.5 cm^2) with calculated specifications of $\varepsilon \approx 0.01$ cm^2 and $\Delta E_n/E_n \approx 4.2$ % [25]. An upgrade of the JET spectrometer was also investigated through simulations and showing an improvement in ε to 0.063 cm^2 but at a cost of degraded energy resolution to $\Delta E_n/E_n \approx 4.7$ % [26].

For NES diagnosis of D plasmas, the count rate capability (C_n^{cap}) of the spectrometer is important to obtain measurement data with good statistical quality. For a TOF spectrometer, C_n^{cap} is, in part, limited by the event rate that the target detector can handle before it saturates and/or the accidental

rate in the t_{TOF} spectrum. For the JET spectrometer, the saturation point was estimated to 6×10^6 Hz from which a $C_n^{cap} \approx 20$ kHz [27] was derived. In the JT-60 case, the saturation point was determined to 2×10^5 Hz [28] indicating a C_n^{cap} in the range of a few kHz. To achieve higher ε and C_n^{cap} values, a new generation of TOF spectrometers is needed, optimized for high count rate as a specific design objective. Accordingly, the TOF spectrometer for Optimized Rate (TOFOR) was developed and built for use at JET. The design target for the TOFOR spectrometer was to achieve $C_n^{cap} \approx 300$ kHz for $\Delta E_n/E_n \approx 6.0$ % and $\varepsilon \approx 0.12$ cm^2.

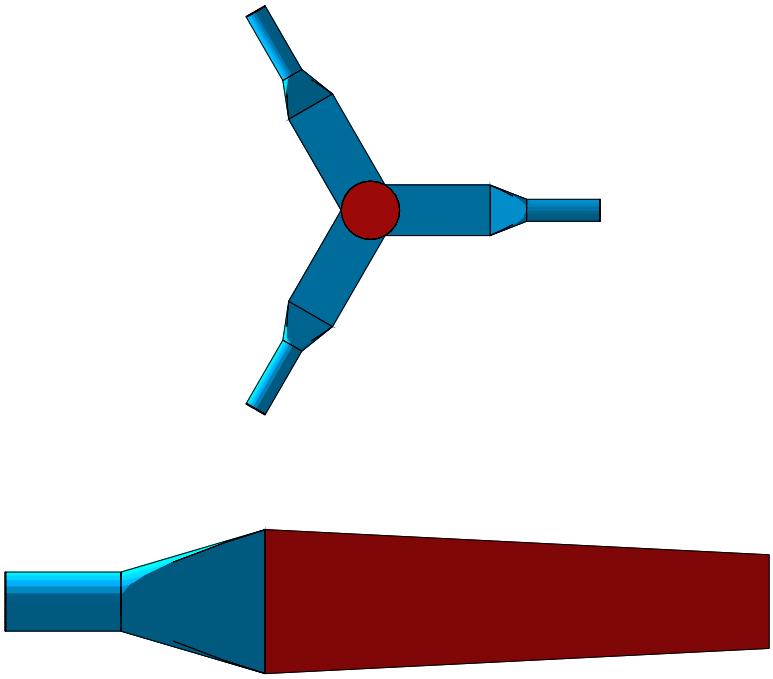

Figure 3.3: S1 (top) and S2 (bottom) detector elements with light guides. A S1 element consists of a circular scintillator (diameter 40 mm, thickness 5 mm) and three attached light guides, each S2 element is a trapezoidal scintillator (length 350 mm, thickness 15 mm, top 95mm and base 134.7 mm) with one light guide attached to the base.

3.4 TOFOR geometry

To handle high count rates, the target detector (S1) in TOFOR was split into five individual scintillator elements of cylindrical shape with a diameter of 40

mm and a thickness of 5 mm. Each element is coupled to three PM tubes via light guides which are glued to the scintillators' circumference. The second TOFOR detector (S2) is built up by 32 identical detector elements to cover a large solid angle relative S1. Each of the S2 elements has a length of 350 mm and a trapezoidal shape with a top of 95.0 mm, base of 134.7 mm and a thickness of 15 mm. At the base, a light guide is connected whose other end couples to a PM tube. The two types of detector elements with light guides are shown in Fig 3.3.

The geometry of TOFOR, is based on a system symmetry axis which goes through the center of S1 and is perpendicular to the circular surface. The incoming beam is also aligned accordingly through the neutron collimator whose axis is that of the system. The S2 detector elements form a ring around the symmetry axis and the center coordinates of the scintillator are located on the constant TOF sphere, of radius $R = 704.6$. The length of the S2 elements cover an angular interval of $30 \pm 7.1^\circ$ relative the S1 detector. With the use of only one PM tube at the base for each S2 detector element, there is a propagation time difference of 2.4 ns for the light produced at the close and far ends of the scintillator relative the PM tube. To compensate for this effect on the t_{TOF} spectrum, each S2 element is rotated around its center coordinates resulting in shorter and longer flight paths for small and large neutron scattering angles, respectively. Hence the neutron flight time will be reduced or increased. Optimizing to 2.5-MeV incoming neutrons, a rotation of 5° reduced the total flight time (neutron flight + light propagation time) over the length of the S2 elements to 1 ns.

3.5 TOFOR digital time recording system

With the recent progress in electronics it is possible to acquire data at high rates (GHz) and to store large quantities of data (GB). Free running time digitizing (TD) cards for use in computers were developed and built for TOFOR [29]. The cards provide one channel for each of the five S1 detector elements and thirty-two channels for the S2 detector elements. The TD cards can digitize the time of signals at a peak event rate of 1.25 GHz/ch with a time resolution of 400 ps which is also the dead time. A maximum of 8 Mevents/ch can be stored in the on-board memory. This would allow time marks to be recorded for a time period well beyond the one minute limit needed for a JET discharge and an event recording rate of 1 MHz/ch for 8s[1].

The data used for the off-line construction of t_{TOF} spectra consist of two time stamp tracks forming a register of events for the detectors S1 and S2 as function of clock time (t_c), i.e, $t_1(t_c)$ and $t_2(t_c)$ as illustrated in Fig. 3.4. Since, the TD cards are free running, they will be open for the entire duration of a

[1]The detectors can also record background radiation which was outside the scope of the thesis

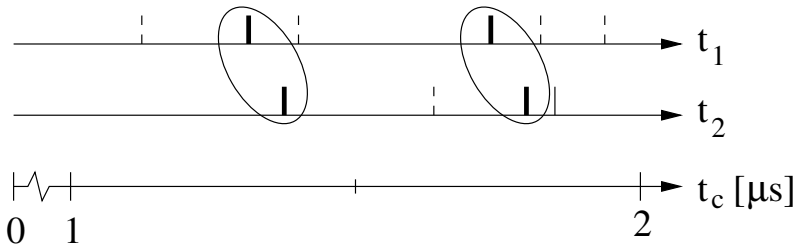

Figure 3.4: Illustration of recorded times (t_1 and t_2) for neutron signals in the detectors S1 and S2 as function of clock time (t_c). The thick ticks (circled) belong to coincident S1 and S2 events and dashed ones are due to uncorrelated neutrons; double recording is indicated with thin ticks.

plasma discharge and record both real neutrons going through both S1 and S2 as well as those passing only one of them.

It is not possible to know *a priori* which of the registered event pairs are due to a single neutron and which belong to two independent neutrons (accidentally paired events). However, there can be no physical events with a negative TOF value (i.e., $t_2 - t_1 < 0$), so this region of the constructed t_{TOF} spectrum can be used to determine the event rate level of accidentals. The t_{TOF} spectra of special interest are those which contain the $t_2 - t_1$ pairs of neutrons in the energy region of $E_n = 1$ to 5 MeV corresponding to flight times in the range 103 to 46 ns, $\delta t_{TOF} \approx 60$ ns. The t_{TOF} spectrum is therefore typically constructed from time pairs where those events recorded in S1 occur within a time span greater than 60 ns (say 200 ns) preceding each event in S2. This t_{TOF} spectrum contains accidental events at the same level as determined separately containing no real coincidences as described above. This means that the admixture of accidentals in the measured t_{TOF} can be accounted for to a high degree of accuracy. The problem with accidentals that affects the neutron TOF spectrum is no longer the same limiting factor as it was with the use of conventional time-to-digital converters (TDC). With these TDCs the range of the time $t_2 - t_1$ difference values of accepted events was selected based on a coincidence window of the electronics and possibly could a separate one be used to determine accidentals only. In both cases, the window settings was fixed before the recording of a discharge. With the new TD electronics, the coincidence windows are applied in the data reduction phase and can be adjusted to suite the purpose or condition at hand.

4. Neutron transport calculations

The realization of the TOFOR spectrometer required extensive neutron transport calculations. First, these were used in the design phase in order to reach, as close as possible, an optimized design to handle high count rates. Second, the measurement data of TOFOR are in the form of t_{TOF} spectra which need to be related to the energy distribution of the neutron flux $F_n(E_n)$ from the plasma. The relationship between the measured t_{TOF} and $F_n(E_n)$ is given by the instrument's response function. It can be divided in two parts, the pulse response (R_p) for given deposited proton energy in the scintillators for a n+p scattering. The second part is the neutron response (R_n) which describes the history of neutrons that enter TOFOR and produce n+p scattering signals. The total response is given by a folding of R_p and R_n where R_p requires empirical input to be determined including that from the operating experience. The neutron response function R_n is simulated with the help of the neutron transport calculations. The major part of this thesis is devoted to the neutron transport calculations of TOFOR, based on Monte-Carlo calculations with the GEANT4 code [30].

4.1 Calculations for TOFOR design

For the TOFOR design, neutron transport calculations were used to quantify the relative importance of different design parameters. The most important parameters to consider are the sizes and shapes of the different scintillator elements (S1 and S2). Moreover, with the use of Monte-Carlo calculations, in the design phase, higher order effects such as neutron multiple scattering in the scintillators themselves as well as surrounding construction material are taken into consideration. A few of the design parameters had to fulfill certain constraints. For instance, the S1 detector elements should have a cylindrical shape, for symmetry reasons, and the S2 scintillator elements should be flat and large with only one PM tube attached to each.

With the use of flat S2 scintillator elements, the solid angle coverage relative the S1 detector must be restricted in order to obtain a spectrometer with acceptable energy resolution. Hence, the neutron scattering angle (α in Fig. 3.2) was restricted to an angular interval ($\pm\theta$) around a mean scattering angle α_m. Moreover, for n+p elastic scattering the pulse height, $P(E_p)$, produced in the scintillators can be expressed as a function of the energy deposited by the recoil proton E_p which is proportional to $\sin(\alpha_m \pm \theta)$. Hence, the choice of

$\alpha_m \pm \theta$ will have a direct consequence on the produced pulse height from a PM tube. With consideration to the light propagation time from the production point in the scintillator to the PM tube and the minimum acceptable E_p[1] in S1, a neutron scattering range of $\alpha_m = 30 \pm 7.1^\circ$ was chosen.

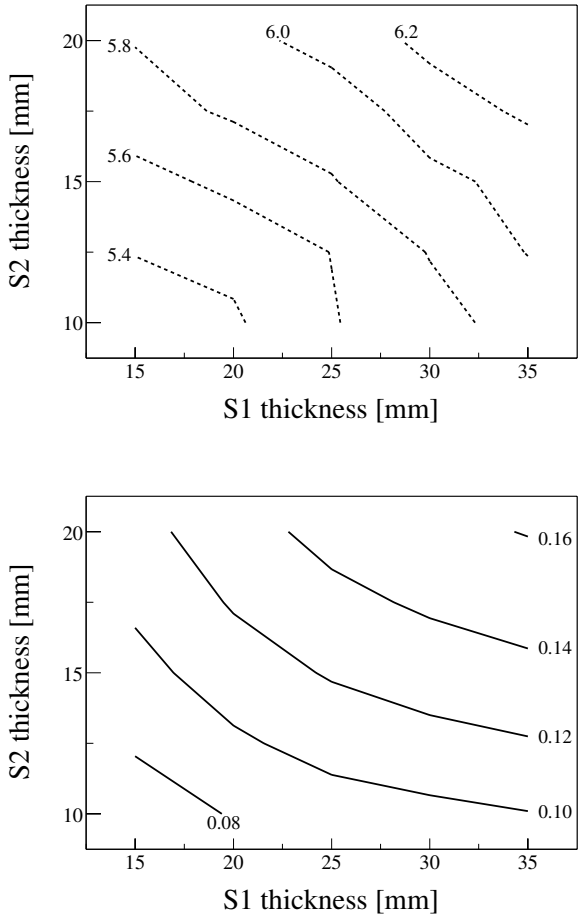

Figure 4.1: Contour plot of simulation results on energy resolution, $\Delta E_{TOF}/E_{TOF}$, and detection efficiency, ε, as function of S1 and S2 thickness. The contours in (a) represents $\Delta E_{TOF}/E_{TOF}$, in the range 5.4 to 6.2 % and in (b) ε from 0.08 to 0.16 cm^2. The numbers shown next to the contours is the $\Delta E_{TOF}/E_{TOF}$ and ε value for that specific contour.

The radius R of the TOFOR constant TOF sphere was taken from the conceptual assessment of a high count rate neutron TOF spectrometers for deuterium fusion plasmas as outlined in Ref. [9]. The design was driven by the ob-

[1]The minimum E_p depends on the required pulse height resolution which in turn is related to the statistical fluctuation in the number of photo-electrons produced in the PM tube.

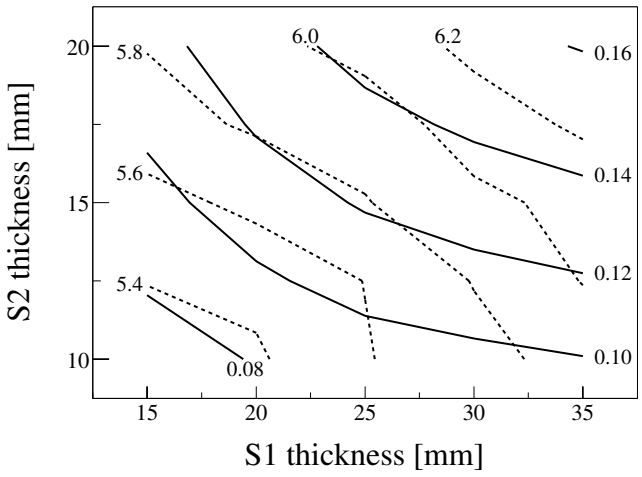

Figure 4.2: Contour plot of simulation results to obtain optimum combination of S1 and S2 thickness for a certain energy resolution. The contours represents energy resolution $\Delta E_{TOF}/E_{TOF}$ (dashed), in the range 5.4 to 6.2 % and efficiency, ε (full), from 0.08 to 0.16 cm^2. The numbers shown next to the contours is the value for that specific contour expressed in % and cm^2 for $\Delta E_{TOF}/E_{TOF}$ and ε, respectively.

jectives to produce a spectrometer with a high count rate capability, C_n^{cap}, high detection efficiency, ε, and an energy resolution, $\Delta E_n/E_n$, suitable to study plasmas with an ion temperature of a few keV. The latter would produce a Doppler broadening width of the neutron emission of 6.6 % so this would set the target energy resolution to the same, i.e., $\Delta E_n/E_n = 6.6$ % (FWHM). This would require a time resolution of or $\Delta t_{TOF}/t_{TOF} = 1/2\Delta E_n/E_n = 3.3$ % with contributions from both R_p and R_n. Allowing R_p for 1.5 % (1 ns for $t_{TOF} \approx 65$ ns for 2.5-MeV neutrons) would set the target value for R_n at $\Delta t_{TOF}/t_{TOF} = 2.9$ % or $\Delta E_n/E_n = 5.8$ % (obtained by quadratic summation).

One of the first neutron transport calculations performed in the design phase of TOFOR was on how the thickness of the different detectors will influence $\Delta E_n/E_n$ and ε of the spectrometer for 2.5-MeV incoming neutrons. With all other design parameters fixed, calculations were performed to predict $\Delta E_n/E_n$ and ε as function of the thicknesses of S1 and S2. The obtained result are shown as contour plots in Fig. 4.1a and b for $\Delta E_n/E_n$ and ε, respectively. For a required E_n resolution, the combination of detector thicknesses that can be used can be read out from the results shown in Fig. 4.1a. As can be seen, only combinations of thicknesses with a intersection point below the $\Delta E_n/E_n = 5.8$ % contour in Fig. 4.1a are allowed. This restriction, in turn, defines the maximum ε that can be obtained with the spectrometer. The contours of constant ε from 0.08 to 0.16 cm^2 as function of S1 and S2 thicknesses are shown in Fig. 4.1b. From the combined contour plots in Fig. 4.2 one can determine how to chose S1 and S2 detectors to obtain optimum efficiency for given resolution.

The maximum contour of ε that is below the 5.8 % energy resolution contour is $\varepsilon = 0.12$ cm^2. Thus, the best combination of thicknesses, for an energy resolution of ≤ 5.8 %, would be around 25 mm for S1 and 15 mm for S2.

As discussed in Sec. 3.3, a limiting factor for the count rate capability, C_n^{cap}, of a TOF spectrometer is the saturation count rate point for the target detector (C_{S1}^{max}). For the type of plastic scintillation detector used in TOFOR, the limit can be set to approximately 2 MHz. With this C_{S1}^{max} value for a 25 mm S1 scintillator, the calculations gave the result of $C_n^{cap} \approx 55$ for 2.5-MeV incoming neutrons. The TOFOR design makes use of 5 identical detector elements of 5 mm thickness, which increases C_{S1} five times raising the estimated C_n^{cap} value up to about 300 kHz. This should be about the count rate level that TOFOR could reach at the maximum theoretical neutron production at JET.

In summary, the design entails the following specifications and target values; five S1 detectors with thickness 5 mm and an area of 12.5 cm^2 each; thirty-two trapezoidal S2 detectors with a thickness of 15 mm, length of 350 mm, 95 mm top and 134.7 mm base (total area of 1.1×10^4 cm^2); a radius of the constant TOF sphere of 704.6 mm with an angular neutron scattering interval of $30 \pm 7.1^\circ$; local energy resolution of $\Delta E_n/E_n \approx 6.0$ % (FWHM)[2]; flux detection efficiency of $\varepsilon \approx 0.12$ cm^2 at $E_n = 2.5$ MeV; count rate capability of $C_n^{cap} \approx 300$ kHz.

4.2 Response function calculations

To produce a response function for TOFOR, a precis model of the spectrometer must be implemented in the simulation code including the scintillators and all large support structures as well as the mechanical structures for the detector assemblies. The model is shown in Fig. 4.3 with some details discussed in Ch. 5.

The TOFOR simulation model treats neutrons interacting in different parts of the system, namely, the active volumes of the scintillators, the material nearest the scintillators (consisting of the light guides and the atmospheric air) and the external material in the form of support structures and PM tube assemblies besides the thin aluminum foils before and after the S1 scintillators. For the interactions in the active detector volumes, the stored data include information on time, interaction position and recoil proton energy.

The response calculations were performed for neutrons in the energy range $E_n = 1$-5 MeV in steps of 50 keV. The neutrons within each bin (i.e, an open interval of [-25,25[in units of keV) were uniformly distributed around the center value E_0 and covering in total, the energy range $E_n = 0.975$ to 5.025 MeV. This was done in order to account for features such as resonances in the neutron cross-sections. The use of finite energy intervals implies some

[2]It can be noted that the local energy response function R_n is valid for mono-energetic neutrons, and can by specified by its neutron time-of-flight or energy

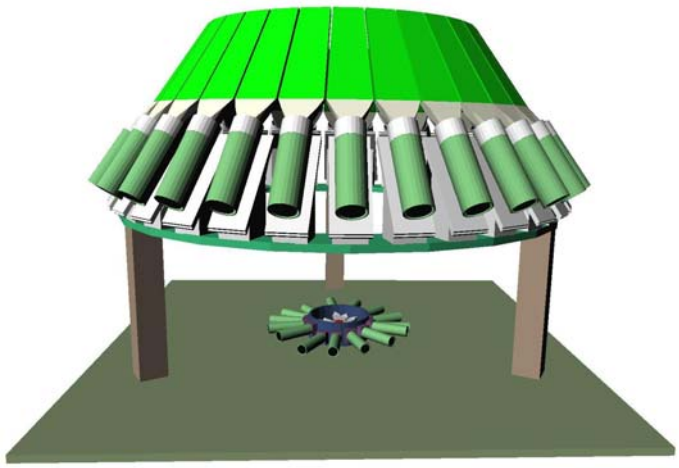

Figure 4.3: Simulation model for response function calculations of TOFOR. Included are the two types of detectors together with their assembly structures. Also shown is the mounting support structures for the spectrometer. Not shown some mechanical structures close to the S1 detector area.

broadening of the calculated t_{TOF} distribution and, hence, effects on the deduced energy distribution, but at a level that is $\Delta E_n/E_n \approx 0.5$ % (FWHM) for $E_n = 2.5$ MeV compared to that for the mono-energetic case.

The end result of the response function calculations for TOFOR is given as a 500×81 matrix in $t_{TOF} - E_n$. It was determined from the t_{TOF} spectra obtained from the neutron transport calculations performed for the 81 energy bins of incoming neutrons. The resulting response function is presented as a density distribution in the $t_{TOF} - E_n$ plane in Fig. 4.4. Here one can see a crescent shaped region ($t_{TOF} \propto 1/\sqrt{E_n}$) of high event density given mostly by neutrons that have only interacted, through n+p scattering, once in the S1 and S2 detector (direct neutrons). The tails to the left and right of the crescent are from neutrons which have interacted more than once in the S1 or S2 detector or in some other structure on their way into S1 or from S1 to S2 (indirect neutrons); the latter situation is also referred to as neutron multiple scattering representing higher order terms in the t_{TOF} spectrum.

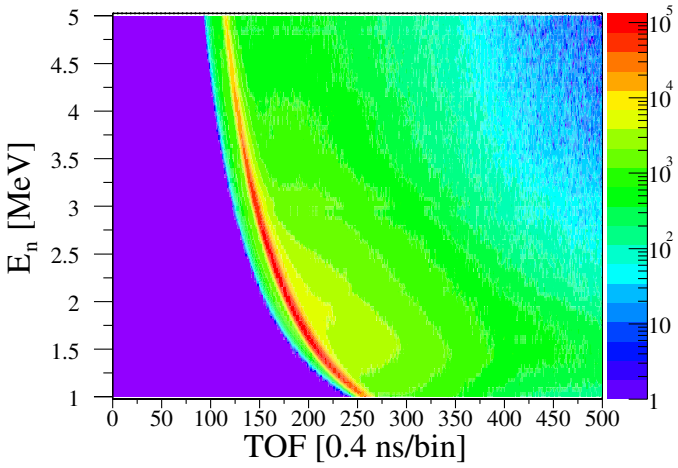

Figure 4.4: Example of the calculated density distribution of the TOFOR response function matrix in the $t_{TOF} - E_n$ plane. Shown is a crescent with high event density mostly form direct neutrons and the tails to the left and right are mostly form indirect neutrons.

5. TOFOR construction and installation at JET

The TOFOR support structure was mainly made from aluminum. It consists of a triangular base plate of 1422.2 mm sides and a thickness of 25 mm. The base plate is also equipped with three adjustable floor legs for alignment purposes. The five S1 detector elements, together with a light tight enclosure, are mounted directly on the base plate. Each of the five S1 detector elements consists of a circular scintillator (Bicron BC-418), three light guides (Bicron BC-800) and three PM tubes equipped with μ-metal for magnetic shielding. To improve the shielding of the PM tubes and hold them in position, each one is placed in a cylindrical tube made of soft-iron which is mounted onto the base plate. A picture of the S1 detector mounted on the base plate is shown in Fig. 5.1.

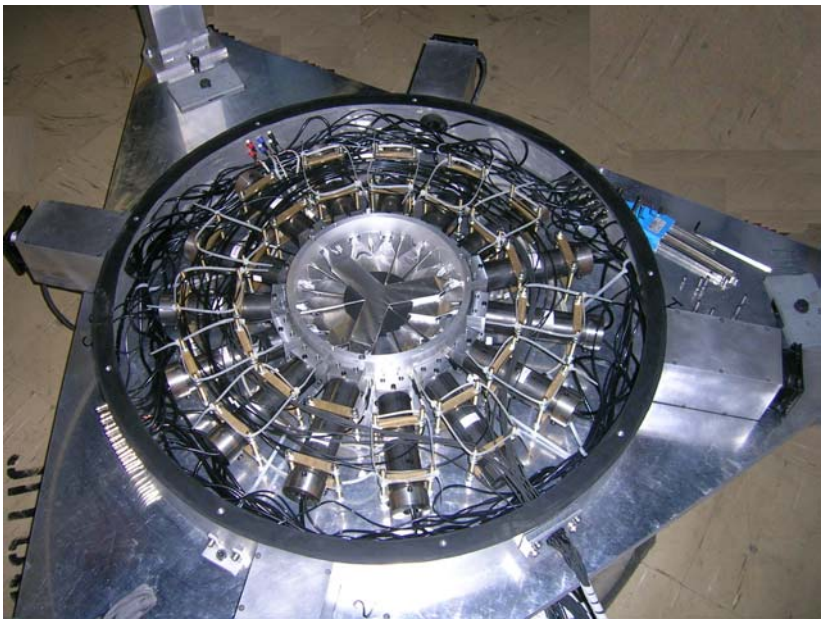

Figure 5.1: Photograph of the final setup of the S1 detector elements. The main parts shown are, the S1 scintillator elements with light guides, wrapped in aluminum and PM tube holders mounted to the base plate.

Figure 5.2: Photograph of TOFOR installed in the roof laboratory at JET showing the triangular base plate, the S1 light tight enclosure, the S2 support ring with mounted S2 detector elements.

The S1 detectors were aligned to the center of the base plate by the crossing of two wires between four reference points. Moreover, the S1 detector elements were mounted so that the scintillators' circular areas are parallel to the base plate. Hence, the base plate and the S1 detectors will be aligned perpendicularly to TOFOR's symmetry axis. In this way the alignment of the S1 detector relative to the base plate and the symmetry axis was estimated to have an lateral accuracy of ± 0.1 mm.

Also attached to the base plate are three legs on which the S2 support ring (radii 700.0 and 861.5 mm and 25 mm thick) is mounted. The S2 support ring is equipped with 64 alignment holes and 64 threaded bolt holes used for fixing the S2 detector holders into position. To obtain high accuracy in the alignment, the detector holders and the support ring are made to a relative position accuracy of ± 0.025 mm. For the alignment of the S2 support ring relative to the center of the base plate and the S1 detector a cross hair was used.

The S2 system consists of 32 detectors of Bicron BC-420 scintillators with attached light guide coupled to a PM tube. Each such detector was an assembly unit which was placed in the holder for the mentioned ring support. During the assembly of the 32 S2 detector elements (scintillator, light guide, PM tube and detector holder), a mounting jig was used to obtain good alignment between the 32 detector elements in terms of position (hight and tilting angle). In this way all 32 S2 detector elements are identical and can be mounted on any position in the S2 support ring with an accurate alignment to the base plant and the S1 detector.

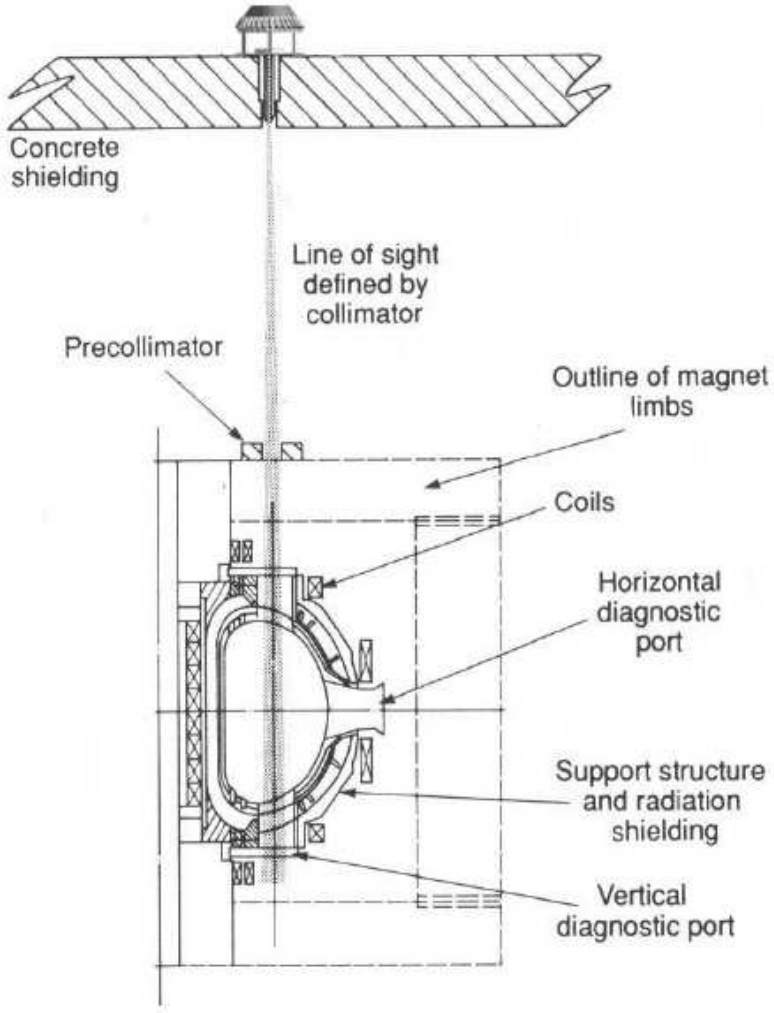

Figure 5.3: Vertical TOFOR line-of-sight from the instrument position in the roof laboratory through the JET plasma core. The line-of-sight is defined by the 1.90 m collimator through the torus hall ceiling.

The construction of TOFOR as outlined above, constitutes an instrument that consists of a number of assembly parts and modules, namely, the base plate with mounted S1 detector, the S2 support ring and the 32 S2 detector elements. This made it possible for easy assembly and disassembly of TOFOR. After construction TOFOR was first assembled and tested in Uppsala. Later it was disassembled into modules for transport to JET and reassembled in the JET roof laboratory (Fig. 5.2).

In the roof laboratory, the TOFOR line-of-sight is defined by a 1.9 m neutron collimator (circular cross section of 12.5 cm^2) passing through the roof laboratory floor having a tilting angle of 0.935° from the vertical line (Fig 5.3). The lateral alignment of TOFOR to the neutron collimator was achieved by the use of the four reference points in the base plate resulting in an alignment accuracy of 0.76 mm of the S1 base plate relative the collimator. Moreover, the base plate was aligned relative to the TOFOR line-of-sight, as defined by the collimator, within $< 0.1^\circ$ by adjusting the height of the three floor legs. Finally, the survey of the S2 support ring showed that it was aligned relative the line-of-sight with $< 0.02^\circ$ with a lateral deviation of < 3 mm. These alignment values was within tolerance and will not have any practical effect on the measuring accuracy of TOFOR.

6. First results from TOFOR

The first fusion neutrons were observed with the TOFOR spectrometer November 1, 2005, from JET discharge #64289. This plasma produced a total of 3.5×10^{14} neutrons of which 140 were detected in TOFOR. At the time for this measurement only one out of five time digitizing cards were in operation which meant that the detection efficiency was only 1/20 of the total normal value. The recorded event distribution as function of the $t_2 - t_1$ time difference is shown in Fig. 6.1 where one can see a peak located around channel #215 which is ascribed to 2.5-MeV dd neutrons coming through the collimator from the D plasma. There are low level tails on both sides of the

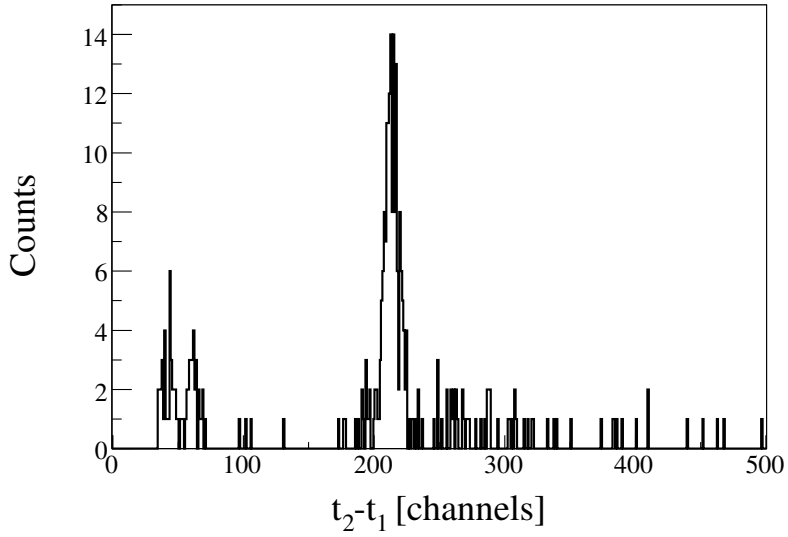

Figure 6.1: The first measured t_{TOF} spectrum by the TOFOR spectrometer from the d+d $\rightarrow$ ^{3}He+n fusion reaction. Shown is the neutron peak located at channel 215 and two small peaks at channel 40 and 60 corresponding to cosmic muons and γ-rays, respectively.

peak, partially, reflecting the presence of neutrons with indirect trajectories on their path from the S1 to the S2 detector. It can also be noted that the spectrometer was operating at a low event count rate. This is consistent with the observation that there are almost no spurious counts in the channel range 80 to 120 which is unphysical for dd fusion neutrons.

A conspicuous feature is the double peak at channel numbers 60 and 40. The peak at 60 is ascribed to γ-rays which come from the plasma through the collimator. These can suffer Compton scattering in S1 and reach S2 after a flight time L/c. The other peak is due to relativistic cosmic muons which have passed through both detectors but in the opposite direction so they appear at lower $t_2 - t_1$ value than γ's and with an apparent negative t_{TOF} of $-\mathrm{L}/c$ (see below).

These observations provided the first confirmation that the TOFOR system was operational and performs as planed in the tokamak environment. Of special importance was to obtain $t_2 - t_1$ data that showed a clear neutron peak in the expected place for d+d $\rightarrow$ ^{3}He+n reactions and an otherwise clean spectrum free of spurious events. It thus performed as envisaged but for the unexpected observations of clear peaks of muons and Compton scattered γ's. Especially, the latter was realized to be of special importance for the time calibration of $t_2 - t_1$ data as it can provide the off-set δt from $t^{\gamma}_{TOF} = t_2 - t_1 + \delta t$ where $t^{\gamma}_{TOF} = \mathrm{L}/c$. In other words, the Compton scattering γ peak would provide a means for an absolute calibration of the $t_2 - t_1$ data whose scale factor ns/ch is given to high accuracy by the specifications of the TD cards.

Commissioning of the TOFOR spectrometer with fusion neutrons was performed with a number of plasma discharges of different heating scenarios in April 2006. From these measurements, the time intervals corresponding to the Ohmic phase of the discharges were selected and summed together in order to get better statistics for analysis. The recorded data in the form of $t_2 - t_1$ distributions were calibrated with the γ-peak as described above to construct t_{TOF} spectra such as the example shown in Fig. 6.2. The neutron part of the spectrum was fitted with a preliminary total TOFOR response function (R_T) which was folded with a Gaussian representing the spectrum of the incoming neutron flux $F_n(E_n)$; R_T was fixed and the width of $F_n(E_n)$ was varied. The fit gives a good description of the recorded neutron spectrum over the neutron peak region including the tail of long flight times. The best fit gave a width for the neutron energy distribution of $\Delta E_n = 149$ keV (FWHM). From the relationship between ion temperature and width ($\Delta E_n = 82.5\sqrt{T_i}$ in keV), we derived an ion temperature of $T_i = 3.3$ keV with an uncertainty of about ± 1.2 keV due to statistics of about 400 counts in the peak. It can be noted that the uncertainty was increased by a factor of 2 compared to what it had been with an instrumental resolution that was lower than the thermal Doppler broadening or 20 % higher than with the target value[1]. Of importance to note here is that the derived T_i value, within the uncertainty, is reasonable for the typical JET conditions at hand. This supports that the assumed R_p value is reasonable and that it can be improved based on the γ-peak width which will be characterized as more data are collected.

[1]The systematic errors in the (absolute) T_i determination with the preliminary response function used can be estimated to better than ± 10 %

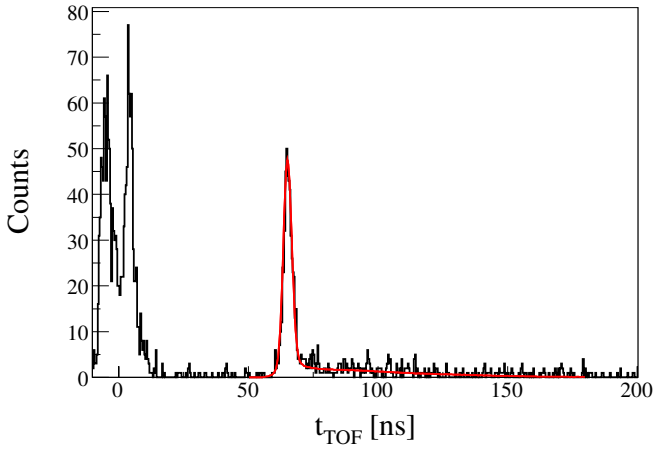

Figure 6.2: Measured t_{TOF} spectrum obtained with TOFOR for the Ohmic phase of the plasma discharges produced during TOFOR commissioning. Also shown is a fit to the neutron peak, obtained with the use of a preliminary TOFOR response function folded with a Gaussian representing the energy spectra of the neutron emission.

With the use of Eq. 3.5 in Sec. 3.2 and a local [2] interpretation of the response function, the t_{TOF} spectrum can be expressed as function of quasi neutron energy, E_{TOF} (Fig. 6.3). A Gaussian fit to the neutron peak gives a width of $\Delta E_n = 292$ keV. This can be taken to have contributions from the neutron and pulse response functions besides the thermal Doppler broadening which is determined through

$$\Delta E_D = \sqrt{\Delta E_n^2 - \Delta E_{R_n}^2 - \Delta E_{R_p}^2}. \tag{6.1}$$

assuming all contributions to be Gaussian. With the use of $\Delta E_{R_n} = 157$ keV from the simulations, and an estimated value of 190 keV for ΔE_{R_p}, one obtains $\Delta E_D = 157$ keV, corresponding to $T_i = 3.6$ keV. This value is slightly higher than the above result which is interesting to discuss from the principle point of view.

The first results on T_i was obtained with the TOFOR response function considering the contributions from neutrons of any energy in the range 1-5 MeV of which those of E_{TOF} values around the peak in the measured t_{TOF} spectrum are the main contributors. This method also allows one to perform fits and analysis of broader complex neutron emission spectra as will be demonstrated in the next section.

In the second case, a local approximation for the response function was used, the width ΔR_n of the calculated t_{TOF} spectrum at $E_n = 2.5$ MeV. Clearly, it can at best only be used for narrowly peaked neutron emission spectra such

[2] Local means that the relationship between E_n and t_{TOF} is for one spectral energy, i.e., $E_n = 2.5$ MeV in this case.

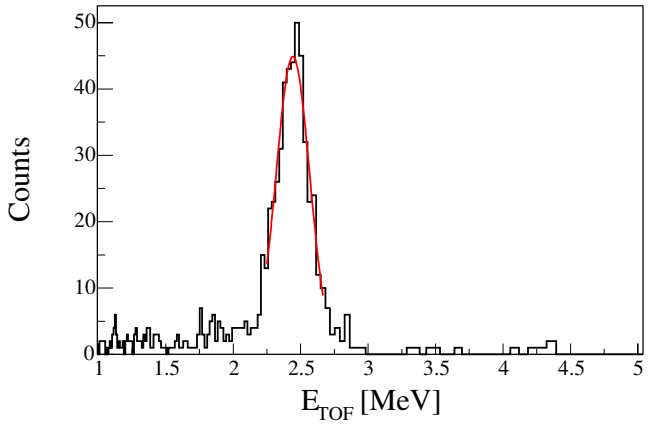

Figure 6.3: Quasi neutron energy spectrum given by Eq. 3.5 and the measurement result of t_{TOF}. Also shown is a Gaussian fit to the peak from which the plasma ion temperature can be determined.

as for Ohmic discharges. Even so, the local response is an approximation valid for mono-energetic neutrons and the width in the present spectrum of 300 keV (i.e., $E_n = 2.5 \pm 0.15$ MeV) is sufficient to give a difference in the result.

The first dedicated experiments was performed with TOFOR in May 2006. The aim was to use NES diagnostics to study the effects on plasmas subjected to RF (ICRH) heating of conditions prepared by NB heating. For these experiments NB beams were injected in the plasma for a couple of seconds. At the point when the beams were reduced, the ICRH power was ramped up to full power and continued so for a few seconds. Here we show examples of spectra acquired during the quasi steady plasma states with NB and NB+RF power injection.

The t_{TOF} spectrum recorded for the NB plasma was fitted with a Gaussian energy distribution for the neutron emission after folding it with the total response function (Fig. 6.4). This gave a fit with a Gaussian width of $\Delta E_D \approx 440$ keV which would correspond to a fictitious bulk temperature $T_B = 28$ keV. Even if the above single neutron emission component describes the gross features of the data, there are regions of deviations around $t_{TOF} = 62$ and 69 ns. These are tale telling features of neutron emission spectrum that is complex.

As the neutron emission spectrum is a reflection of the underlying motion of the deuterons in the plasma, it is reasonable to assume that the population has a bulk Maxwellian velocity component giving a Gaussian neutron distribution as before. In addition, there would be a component representing the supra-thermal ions from the NB injection. These supra-thermal ions have a gyro motion around the magnetic field lines perpendicular to the line of sight

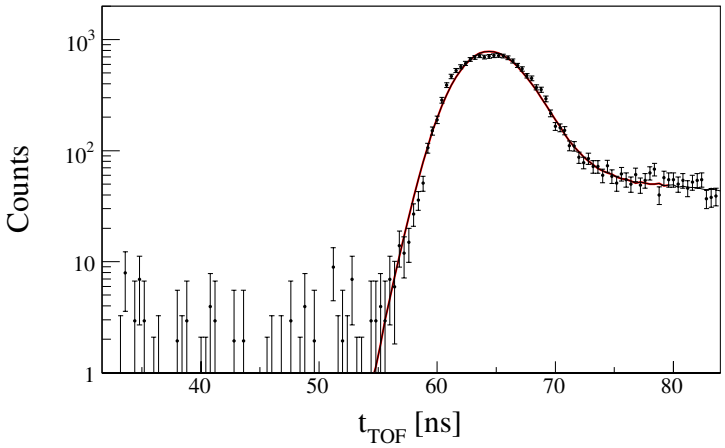

Figure 6.4: The resulting t_{TOF} spectrum collected during the NBI phase of the JET discharge #66459. The line represent a fit to the data with the use of a single component model for the neutron emission.

of TOFOR and give rise to a special (double humped) neutron emission spectrum and a corresponding high energy (HE) signature in the t_{TOF} spectrum. The dual component (bulk + HE) neutron spectrum gives a good description of the observation and no essential features are left out (Fig. 6.5). The width of the Gaussian was varied in this case from which one can extract a bulk temperature $T_B = 16$ keV. It should be noted that T_B is a quasi temperature as the ions contributing are partly non-thermal; they could be represented by a perturbed Maxwellian due to the likely admixture of supra-thermal components from the NB injection.

When RF is applied to the plasma, the result is a drastic change in the neutron emission as shown by the t_{TOF} spectrum recorded with TOFOR (Fig. 6.6). In comparison to the results for pure NB heating (Fig. 6.5), the bulk of the spectrum is much broader. In addition, the spectrum has extended tails which are absent in the NB spectrum. It is clear, that the RF spectrum is complex and the lowest order approximation to describe it is to use a bulk Gaussian and a high energy component coming from the supra-thermal ions generated by the RF interacting with the NB and bulk ions. The RF waves create gyro acceleration of the deuterons resulting in a supra-thermal population described with a Maxwellian of temperature T_{RF}. Such two component fit was used to describe the data shown in Fig. 6.6. It can be noted that the best fit was obtained with a temperature of $T_{RF} = 570 \pm 100$ keV for the supra-thermal Maxwellian. The bulk was found to have a width corresponding to $T_B = 39$ keV taken as the thermal Doppler broadening this T_B value is of course a fictitious temperature as noted already. However, it is interesting to note that the bulk component created with NB+RF is broader than that with NB only

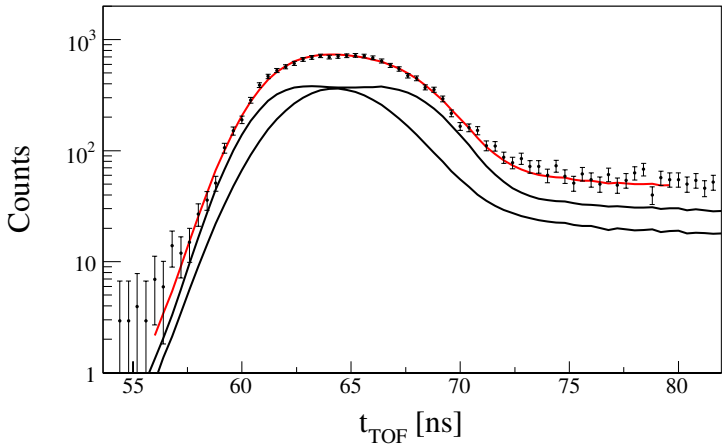

Figure 6.5: The resulting t_{TOF} spectrum collected during the NBI phase of the JET discharge #66459. The line represent a fit to the data with the use of a two component model for the neutron emission.

($T_B = 16$ keV). The physics behind this difference will be an obvious objective for further studies with TOFOR.

The above example shows what was found as a trend in the results of the experiments, namely, that the peak including the tail in the short time region (high neutron energy) is well described by the fits. The region of t_{TOF} values of neutron energies below the peak value of 2.5 MeV is not well described. This region is especially sensitive to the details of the response function as well as the spectrum of the collimated neutron flux from the plasma and its admixture of scattered contributions. However, from the NES diagnostic point of view, it is the high energy side that is the most important. In this respect, the observational capabilities of TOFOR demonstrated, are the quality of the data and the first analysis using a non-local response function. Still, the ability to measure on both sides of the maximum in the t_{TOF} spectrum in order to study and verify the non-locality of the response function. The presented measurements are the first of sufficient quality to consider this aspect and with a matching neutron response function to demonstrate it. This is further discussed in the next section.

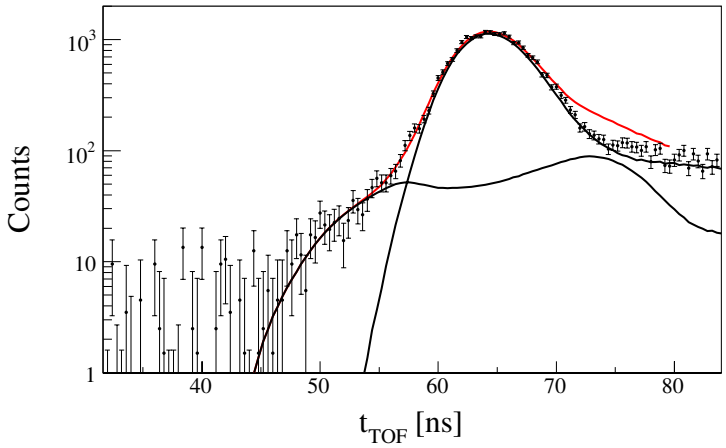

Figure 6.6: The resulting t_{TOF} spectrum collected during the ICRH phase of the JET discharge 66455. The line represent a fit to the data with the use of a two component model for the neutron emission.

7. Discussion, conclusions and outlook

The simulated neutron response function R_n is correct to a high degree with respect to its variation with E_n. Its absolute value, i.e., detection efficiency, depends on its relationship to the number of events in the t_{TOF} spectrum that each detected neutron creates in the simulated and measured spectra. Ideally, there should only be one event per neutron, or, at least the same number in both. The multiple counting effect was partially assessed in this thesis and found to have some effect on the response function. This was fixed by an ad hoc patch to the response function used in the analysis results presented so the remaining effect should be rather insignificant. This means that the neutron part of the response should, for all practical purposes, serve well for the qualitative description of the measured t_{TOF} spectra.

To obtain the total response, one also needs the part that describes the scintillator and electronics response (R_p) to the pulses generated by the E_p values which are an output from the R_n calculations. Here, we have used a Gaussian function with a fixed width, i.e., R_p represents resolution of the measured time difference $t_2 - t_1$. Clearly, this is an approximation as one would expect the time resolution Δt to improve with increased E_p, i.e., pulse height. Moreover, the pulse height resolution ΔV would increase with E_p so that the sharpness of the pulse height discrimination would increase with increasing E_p and, hence, E_n to be poorest for events with E_p near the lower threshold. In short, there are reasons to believe that a fixed value of R_p is only a lowest order approximation and that there should be higher order terms depending on E_n. In other words, the R_p response used here is local in the sense it might only be valid for a certain E_n, say, $E_n = 2.5$ MeV. The total response function that is available now is thus non-local to its neutron part R_n and local to its pulse part R_p.

In chapter 6, the response function was applied to the measured t_{TOF} spectra for NB and NB+RF plasmas which generated very different neutron emission spectra. Especially, both contained a double-humped high energy component but with great difference in energy width. The NB spectrum extends between the half amplitude points $t_{TOF} = 60$ and 62 ns (Fig. 6.5), which, in terms of energies of local response functions correspond to $E_n = 2.9$ and 2.2 MeV, i.e., a spread of 0.3 MeV or of 28 % relative to $E_n = 2.5$ MeV. The same half amplitudes points in the NB+RF spectrum (Fig. 6.6) are $t_{TOF} = 52$ and 72 ns which can be related to local E_n values of 3.9 and 1.7 MeV, respectively, corresponding to an energy spread of 2.3 MeV or 92 % around $E_n = 2.5$ MeV. It is interesting to note that for neutron energy spectra of limited spread (28

%) it is possible to describe the observed t_{TOF} spectrum including the tail region $t_{TOF} > 70$ ns (Fig. 6.5). This is not the case for the wide RF spectrum (Fig. 6.6) where, indeed, there is an over-shoot in the calculation by about 40 % at the location of the right hand peak of the double humped distribution ($t_{TOF} \approx 75$ ns). There can be several contributing factors to the deviation of which the local pulse response function R_p used is one. If the whole difference between prediction and observation at $t_{TOF} = 75$ ns is ascribed to this effect, and assuming that the non-locality of R_p varies linearly with E_n, the local R_p used could be taken to give an under estimation of 20 % at $E_n = 3.9$ MeV and the same over estimation at $E_n = 1.7$ MeV. By the same token, some deviation would also show up in the NB spectrum but would only be 8 % and too small to observe. It is envisage that the analysis of t_{TOF} spectra for narrow and wide neutron energy distributions will be able to determine the non-local R_p function whose general E_n dependence could be obtained on theoretical and empirical grounds.

TOFOR will make it possible to perform NES observations of D plasmas with higher sensitivity to details in the neutron emission than has been possible with earlier generations of 2.5-MeV neutron spectrometers [11]. This derives from a significantly higher (factor of hundred) count rate capability of TOFOR. Thanks to high flux detection efficiency, this can also be exploited for maximum power D plasmas at JET. One can thus expect TOFOR to operate at count rates in the 100 kHz range which gives the counting statistics needed for the observation of the dominant component of the neutron emission with high time resolution (typically $\Delta t_c < 10$ ms) or week components, at say the 1 % level with $\Delta t_c < 1$ s. The weak components appear as high and low energy tails of the main spectral component, typically, centered at $E_n \approx 2.5$ MeV. The region of interest for NES diagnostics has been extended to the range $E_n = 1.5$ to 5 MeV, (paper I), which TOFOR had to be designed for.

The above general goals were transferred into design specifications with the help of early versions of the model and programs for neutron transport calculations developed as part of this thesis. The calculations were also used to simulate the response of TOFOR to neutrons for specific energies in the range 1 to 5 MeV with respect to the observables t_1, t_2, E_{p1} and E_{p2} from which t_{TOF} spectra were constructed as well as their dependence on selection of proton recoil energies. Based on these Monte Carlo calculations, the neutron response function (R_n) has been determined in terms of t_{TOF} spectra for given E_n which is described as a 500×81 matrix depending on the selection of E_{p1} and E_{p2} values.

The R_n matrix would be the total TOFOR response function (R_T) if the four variables could be measured precisely. This, however, is not the case but the signals created by E_p in the scintillators and electronics have a pulse that is a non-linear function of E_p. Moreover, the pulse height and time are measured with finite resolution. These aspects of the TOFOR response (the pulse response function R_p) are not possible to predict with sufficient accuracy to be

useful, but empirical input is needed for determination or, at least, to obtain estimates. Some scintillator tests have been done as reported in this thesis and elsewhere [31] while the final and best input is going to come from analysis of data taken with TOFOR in suitable experiments with fusion neutrons. This is exemplified below.

In lieu of a pulse response function, a Gaussian function has been used to describe the finite resolution by which the $t_2 - t_1$ difference can be measured which, based on different inputs; this time resolution has been estimated to be 2.5 ns (FWHM), or $t^p_{TOF}/t_{TOF} = 2.5/65 = 3.8$ % at $E_n = 2.5$ MeV, while the corresponding value for R_n is $\Delta t^n_{TOF}/t_{TOF} = 3.2$ %. The total response function (local for $E_n = 2.5$ MeV) is estimated by folding R_n with R_p and by quadratic summation one obtains $\Delta t_{TOF}/t_{TOF} = 4.9$ %. The target was to achieve $t^p_{TOF} < 2$ ns which is now considered unlikely to be reached because of lower light collection efficiency than expected in the S1 scintillator [1].

As the pulse time resolution is such a large fraction of the t_{TOF} spectral resolution it will affect the uncertainty by which Δt_{TOF} is determinable. Here, the situation is better than envisaged as the Compton scattered γ's coming through the collimator produce such a clear signal in the TOFOR spectra. In the future, the simulation program will be set up to perform transport analysis of the γ spectra recoded under optimal signal conditions so that the shape can be determined and analyzed to high accuracy. Since $\Delta t^n_{TOF}/t_{TOF}$ is determinable to great accuracy through simulations with the set by the error in Δt^p_{TOF} for which ± 0.1 ns should be attainable. An overall error at the 0.1 ns level would mean, for instance, that ion temperatures of $T_i \geq 4$ keV can be determined with absolute error of less then ± 10 %. The main effect of the lower than expected time resolution is that it would take twice the number of counts to achieve the same statistical accuracy as with the target value resolution.

Measurements of the low amplitude tails in the spectrum means that the response function must be well known, not only to its lowest order but also to its higher order terms. The lower order terms are also referred to as events in the t_{TOF} spectrum due to direct neutrons, with only one basic interaction in S1 and S2. Higher order terms are due to indirect trajectory neutrons involving multiple scattering (MS) which were also calculated and studied in detail in this thesis. This is essential information for a neutron TOF type of spectrometer to be used for broad band energy measurements. Specifically, the MS terms are important as they make a certain fraction of neutrons of different energies show up at the same location in the t_{TOF} spectrum.

The admixture of MS contributions is generally small for energy spectra that are narrow. This allows one even to approximate the response function with the t_{TOF} distribution for one E_n value being the central value of the neu-

[1] With a local response function, $\Delta t_{TOF}/t_{TOF}$ can be expressed as a neutron energy resolution of $\Delta E_{TOF}/E_{TOF} = 2\Delta t_{TOF}/t_{TOF} = 9.8$ %. This energy resolution is equivalent to the Doppler broadening that the neutron emission distribution would have for a thermal plasma of $T_i = 8.8$ keV.

tron emission, i.e., one of the 81 columns of the response matrix. This is a local approximation of the R_n response function and is what has been used in previous analyses of TOF data (see, for instance Ref. [26, 32]). It is often also the basis for describing the performance of a TOF spectrometer by parameters such as neutron energy resolution. However, a local response is not sufficient for analyzing data over large energy bands and it is also not possible to characterize the capabilities of a broad-band spectrometer in simple parametric terms. However, the performance can be demonstrated through its use in actual experiments and in the results obtained from analysis using non-local neutron response such as discussed below.

Based on the achieved neutron simulation characterization of TOFOR, and the initial measurement results obtained, one can envisage some interesting development lines. One is to exploit the continuing progress in the field of electronics which could open up the possibility to develop hybrid cards that can digitize both time and pulse height (and shape) simultaneously. These would be used to record both t and E_p information for the S1 and S2 signals in TOFOR. It would mean that one can eliminate the present use of discriminator electronics to select events in the t_{TOF} spectrum based on having passed upper and lower thresholds. A data acquisition system with hybrid cards would allow event selection based on E_{p1} and E_{p2} values to be made *post mortem*, with adjustability to suit the special features in the t_{TOF} spectrum one wants to focus on. This means that one would not have to truncated the energy range of incoming neutron flux as is the case now with thresholds set for accepted E_{p1} values. Another interesting aspect is the correlation studies between the four variables t_1, t_2, E_{p1} and E_{p2} which means that one has access to all information there is for each recoded signal events in S1 and S2. This can be put to use in different ways. One is to improve the resolution by which the times t_1 and t_2 can be determined. It can also be used to improve the selection of events based on pulse height so that the faction MS event admixture in the t_{TOF} spectrum is decreased. Thirdly, the time difference $t_2 - t_1$ and E_{p1} can be used to further reduce the admixture of MS events. Finally, it can be used in the pulse height calibration of the S1 and S2 detectors. With hybrid cards and a more extensive data reduction, the final result will be a cleaner t_{TOF} spectrum mainly because the MS tails will be reduced. The change of data acquisition could be implemented and used on the existing TOFOR instrument and would mean a better realization of the concept it was based on, namely, to raise the count rate capability of TOF spectrometers. This limit is set by the rate in the S1 detector which in case of TOFOR is reduced by eliminating those E_{p1} values which do not belong to scattered neutrons of expected t_{TOF} value. The hybrid cards would be the platform for the next improvement of the present instrument which can be taken as a prototype, with its response, for the next generation TOFOR spectrometers.

8. Sammanfattning på svenska - Swedish summary

Ett av framtidens stora problem är den ökande konsumtionen av energi. Detta leder till att nya energikällor, antagligen, kommer att bli nödvändiga inom en snar framtiden. En framtida potentiell kandidat för energi produktion är fusion. Fusion är den kärnprocess som driver solen och bygger på att slå ihop kärnor av lätta grundämnen och på detta sätt få ut ett överskott på energi. För att kunna få denna process att fungera på jorden krävs en fusionsreaktor som har förmågan att skapa ett fusions plasma. Detta kan uppnås genom höja temperaturen på fusionsbränslet till hundra miljoner grader Kelvin vilket motsvarar en rörelse energi av 10 keV för bränslepartiklarna. Det vanligaste bränslet som användes inom fusionsforskningen är två väte isotoper, deuterium (d) och tritium (t), vilket ger att i huvudsak tre fusions reaktioner som kan äga rum, nämligen,

$$\mathrm{d{+}d} \rightarrow {}^{3}\mathrm{He} + \mathrm{n}, \tag{8.1}$$

$$\mathrm{d{+}d} \rightarrow \mathrm{p} + \mathrm{t} \tag{8.2}$$

och

$$\mathrm{d{+}t} \rightarrow \alpha + \mathrm{n}. \tag{8.3}$$

I två av dessa reaktioner är en av slutprodukterna en neutron (n) och om mätningar utföras på dessa kan viktig information fås om de fusions processer som pågår inuti reaktorn. I denna avhandling beskrivs de steg som tagits för att bygga ett instrument som kan mäta neutronens rörelseenergin. Med dessa mätningar kan information fås om bränslets temperatur vilket är en av tre parametrar som används för att bestämma om ett fusionsplasma brinner.

Det finns många olika tekniker för att mäta rörelseenergin av de neutroner som producerats i en fusions reaktor. I denna avhandling ligger fokus på en spektroskopisk metod som baseras på flygtids mätningar. I denna metod mäts den tid, t, det tar för en partikel att färdas en sträck, L, mellan två punkter i rummet. Om avståndet L är fixerat och t fås från mätningar, kan partikelns hastighet v beräknas av

$$v = \frac{L}{t} \tag{8.4}$$

med, vilket rörelseenergin E kan fås från

$$E = \frac{1}{2}mv^2 = \frac{1}{2}m_n\left(\frac{L}{t}\right)^2 \tag{8.5}$$

där m är partikelns massa. Detta är den underliggande fysikaliska princip som används för att bestämma rörelseenergin för en partikel med hjälp av en flygtidsspektrometer. Vid användning av denna metod för mätningar av neutroner är det många faktorer som spelar in, vilket gör att det är en komplicerad metod att genomföra.

En faktor som komplicerar genomförandet av neutronmätnigar är att neutronen saknar laddning så direkt detektion kan inte ske. Neutroner måste därför växelverka med ett material eller en partikel och på detta sätt generera laddade partikler som kan detekteras. Den flygtidsspektormeter som avhandlas här bygger på att en och samma neutron växelverkar genom elastisk spridning mot protoner i två olika detektorer. De producerad protonerna detekteras genom att genererar elektriska signaler vars tider t_1 och t_2 för de två detektorena registreras vilket ger neutronens flygtid $t = t_2 - t_1$. I en riktig mätsituation kommer det att vara ett flöde av neutroner som infaller mot spektrometern vilket ger ett slutresultat i form av ett flygtidsspektrum.

En andra faktor som påverkar neturonmätningar är sannolikheten för att en neutronväxelverkan skall äga rum. För att uppnå en hög sannolikhet för neutron spridning och en hög detektions effektivitet i en flygtidsspektometer, måste de detektorerna som används vara av en viss storlek. Detta medför att L i den ovanstående ekvationen för rörelseenergi är en approximation till den flygsträck som en neutron passerar mellan de två detektorerna. Vilket leder till att denna ekvation inte skall användas för att bestämma neutronens rörelsenergi. Istället beräknas en responsfunktion för spektormetern vilken beskriver hur ett flygtidsspektrum skall se ut som funktion av den inkommande neutronernas rörelseenergi. På detta sätt kan ett mätt flygtidsspektrum relateras till rörelseenergin av de inkommande neutronerna. En stor del av arbetet till denna avhandling har att med hjälp av beräkningar försöka bestämma responsfunktionen för en ny flygtidsspektometer.

Acknowledgment

The starting point of this work was during my Diploma thesis in which 2.5-MeV neutron measurements were performed with the MPR spectrometer. This was like looking for a needle in a haystack and the TOFOR idea was born and my PhD studies started. This opportunity was given to my by the Advanced Instrumentation and Measurements (AIM) graduate school, the Swedish Foundation for Strategic Research (SSF) and Jan Källne my supervisor.

First I want to express my deepest gratitude to Jan for his belief in me and all the support he has given me during my years as a PhD student. I also want to thank you for the help I received to understand the art of scientific research, nuclear physics and especially neutron spectroscopy. Finally I want to thank you for the time you spent in order to get the TOFOR project to the point were it is today, thank you.

The TOFOR project is and has been a team work and a lot of people have been involved. The core of the team I rely want to thank, Matthias Weiszflog, thank you, for all the work you have put in to the project, my fellow PhD students Luca Giacomelli and Maria Gatu Johnson, thank you for all discussions and all the questions raised during the time working together on the TOFOR project. Sean Conroy, thank you for the efforts you put into the data acquisition software and all the advise you have given to me in code development and computer games. Thank you Johan Thun for the programing and setting up of the CAMAC sub-system.

The MPRu project has been running in parallel with TOFOR and a lot of common work has been carried out. Therefor I take the opportunity to thank the MPRu crew, Göran Ericsson, thank you for all your suggestions and support during all stages in the projects, Henrik Sjöstrand, Erik Andersson Sundén, Carl Hellesen and Emanuel Ronchi, thank you for the nice working environment and for the enjoyable moments at the pubs and in the house during our trips to JET.

I also want to express my gratitude to the people that have work at INF, IKP and TSL and made it to a great working place, “Bumpen”, Michael, Joakim, Cecilia, Pär, Nils, Angelica, Janne, Martin, Hans, Marco, Luigi, Peter, Staffan, Christoffer, Otas, Ib, and Susanne.

My friends have been a large resource of fun and comfort during the time spent as a PhD student, thank you all, mountain bike friends, golf friends, innebandy friends, student friends, badminton friends, and my childhood friends.

I and certain that I have forgot to mention a lot of people which should have been acknowledge and I sincerely hope that all of you accept my apologies and thank yourself on may behalf.

Till sist vill jag tack min familj för att ni alltid ställt er bakom mina ibland egendomliga idéer och äventyr, Mamma, Pappa och mina storebröder Peter, Mathz och Kjell. Hade ni inte stöttat mig så hade nog detta äventyr slutat i katastrof.

References

[1] A. Peres, J. Appl. Phys., **50(9)**(1979) 5569

[2] U. Stroth, Plasma Phys. & Controlled Fusion, **40**(1998) 9

[3] The JET Team, Plasma Phys. & Controlled Fusion, **32**(1990) 1083

[4] R. Aymar *et al.*, Plasma Phys. & Controlled Fusion, **44**(2002) 519

[5] C. M. Braams *et al.*, Nuclear Fusion - Half a Century of Magnetic Confinement Fusion Research. Institute of Physics Publishing, London (2002)

[6] M. Keilhacker *et al.*, Europhysics News, **26(6)**(1999) 230

[7] A. Lioure *et al.*, JET report, **EFDA-JET-CP(04)06-25**(2004)

[8] J. Källne, EFDA-JET Project Document, **EP-DIA-TOFOR S001-0**(2002)

[9] G. Gorini *et al.*, Rev. Sci. Inst., **63**(1992) 4548

[10] H. Brysk, Plasma Physics, **15**(1972) 611

[11] O. Jarvis, Plasma Phys. & Controlled Fusion, **36**(1994) 209

[12] L. Ballabio *et al.*, Nucl. Fusion, **38**(1998) 1723

[13] J. Frenje *et al.*, Rev. Sci. Inst., **70**(1999) 1176

[14] L. Ballabio, Uppsala University Neutron Physics Report, **UU-NF 95/#7**(1995)

[15] P. Van Belle *et al.*, Basic and advanced diagnostic techniques for fusion plasmas, **III**(1986) 767

[16] J. D. Strachan *et al.*, Nature, **279**(1979) 626

[17] F. Hoenen, Nucl. Inst. & Meth., **233**(1984) 150

[18] M. Pillon *et al.*, Nucl. Inst. & Meth., **B101**(1995) 473

[19] A. Krasilnikov *et al.*, Rev. Sci. Inst., **68**(1997) 1720

[20] B. Esposito *et al.*, Rev. Sci. Inst., **75**(2004) 3550

[21] J. Källne *et al.*, Nucl. Inst. & Meth., **A311**(1992) 595

[22] G. F. Knoll, Radiation Detection and Measurement. Wiley, New York, 3rd edition (1999)

[23] H. Kishimoto *et al.*, Nucl. Fusion, **45**(2005) 986

[24] M. Hoek *et al.*, Fusion Eng. & Design, **45**(1999) 437

[25] M. Olsson, Nucl. Inst. & Meth., **A316**(1992) 395

[26] M. Hoek, Nucl. Inst. & Meth., **A323**(1992) 656

[27] T. Elevant *et al.*, Rev. Sci. Inst., **63**(1992) 4586

[28] Y. Shibata *et al.*, Rev. Sci. Inst., **72**(2001) 828

[29] J. Sousa *et al.*, Fusion Eng. & Design, **71**(2004) 101

[30] S. Agostinelli *et al.*, Nucl. Inst. & Meth., **A506**(2003) 250

[31] P. Magnusson, Uppsala University Neutron Physics Report, **UU-NF 06/#4**(2006)

[32] T. Elevant, Nucl. Inst. & Meth., **A476**(2002) 485

Acta Universitatis Upsaliensis

Digital Comprehensive Summaries of Uppsala Dissertations from the Faculty of Science and Technology 233

Editor: The Dean of the Faculty of Science and Technology

A doctoral dissertation from the Faculty of Science and Technology, Uppsala University, is usually a summary of a number of papers. A few copies of the complete dissertation are kept at major Swedish research libraries, while the summary alone is distributed internationally through the series Digital Comprehensive Summaries of Uppsala Dissertations from the Faculty of Science and Technology. (Prior to January, 2005, the series was published under the title "Comprehensive Summaries of Uppsala Dissertations from the Faculty of Science and Technology".)

Distribution: publications.uu.se
urn:nbn:se:uu:diva-7198

ACTA
UNIVERSITATIS
UPSALIENSIS
UPPSALA
2006